Galaxy: global properties

Parameters of our Galaxy

Distance to the Galactic center	R_0 = 8.0kpc ±0.5
Rotation velocity	V_0 = 230 ±10 km/s
Disk Luminosity in V band	1.2 x 10^{10}Lsun
Bulge Luminosity in V band	2 x 10^{9}Lsun
Disk M/L in V band	4-5
Disk+bulge mass	(5-6) x 10^{10}Msun
Bulge mass	(0.5-1) x 10^{10}Msun
Virial mass	10^{12}Msun
Virial radius	260 kpc
Type	SBb
Disk scale length	Rd = 3.0 ±0.5 kpc
Bulge scale length (R_e in 1/4 law)	2.7 kpc
Bar length	3. -3.5 kpc
Period of vertical oscillations	6.2 x 10^{7}yrs
Rotational period at R_0	2.4 x 10^{8}yrs
Oort limit (density in the plane)	0.11 Msun/pc^3
Solar motion relative to the Local Standard of Rest	13.3±0.8 km/s
Escape velocity at the solar distance	550-570 km/s

Milky Way: GAIA

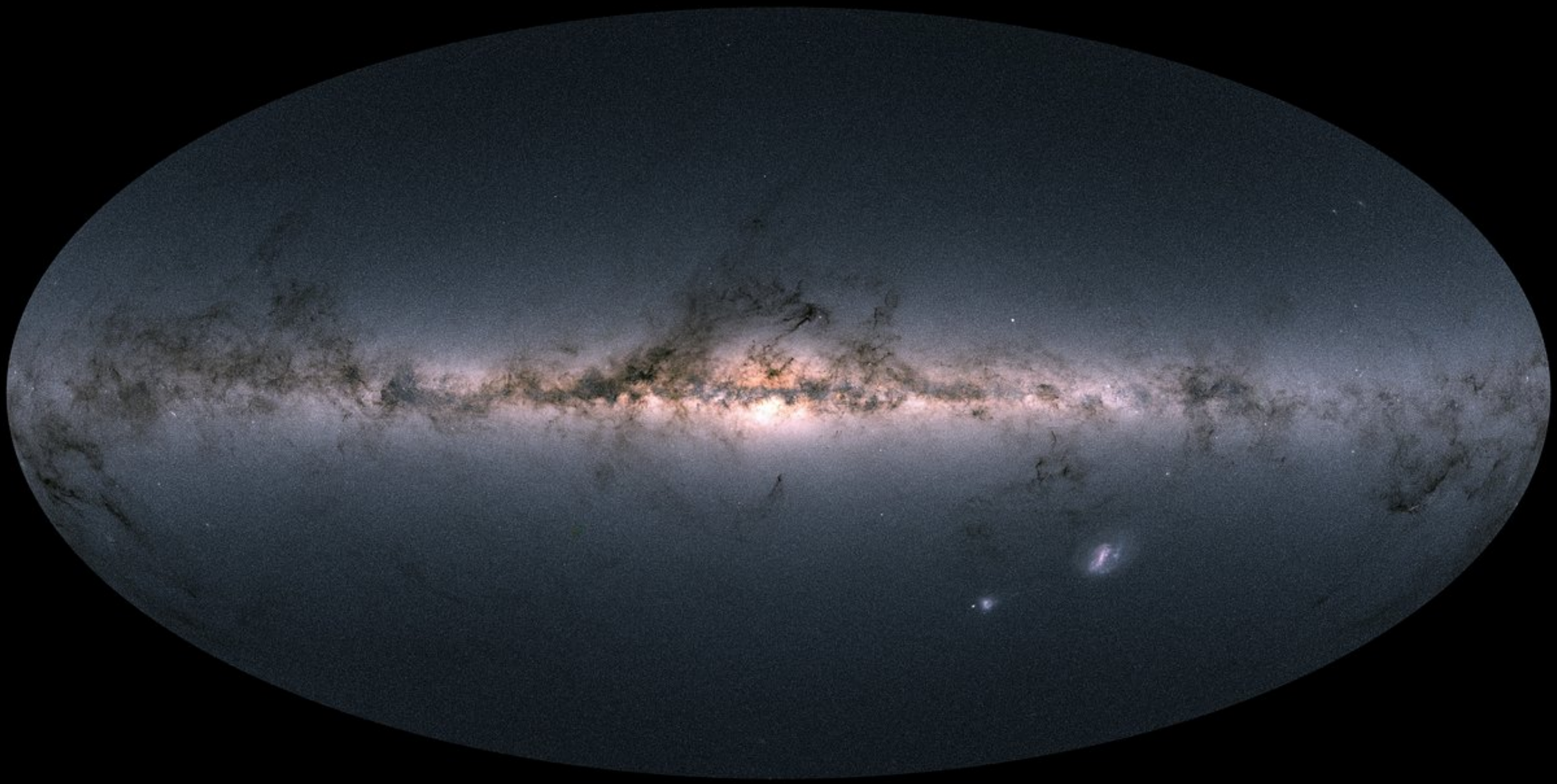

This image shows Gaia's all-sky view of the Milky Way based on measurements of almost 1.7 billion stars.

An all-sky view of the interstellar dust that fills our Milky Way Galaxy, based on observations performed by ESA's Gaia satellite

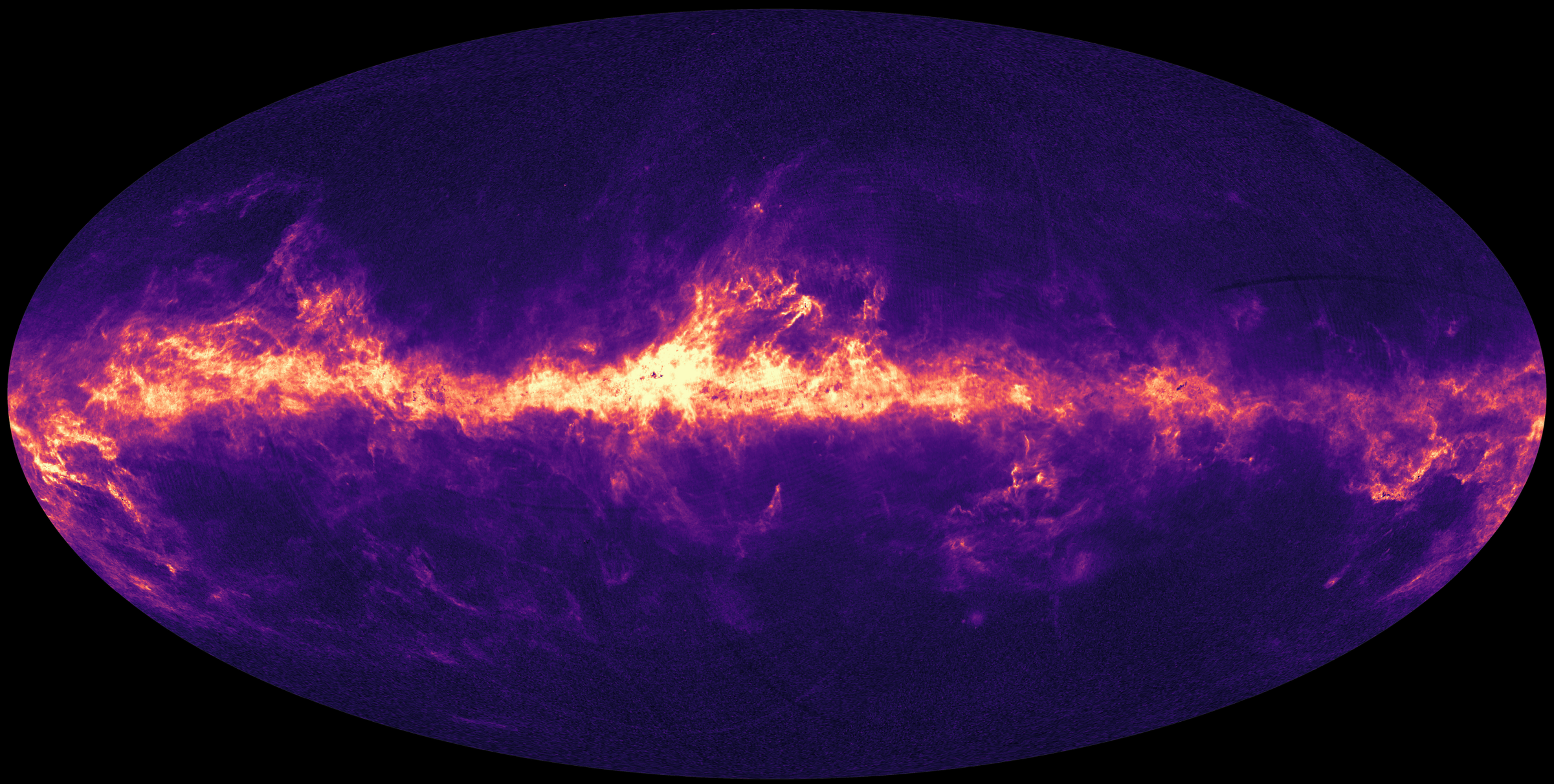

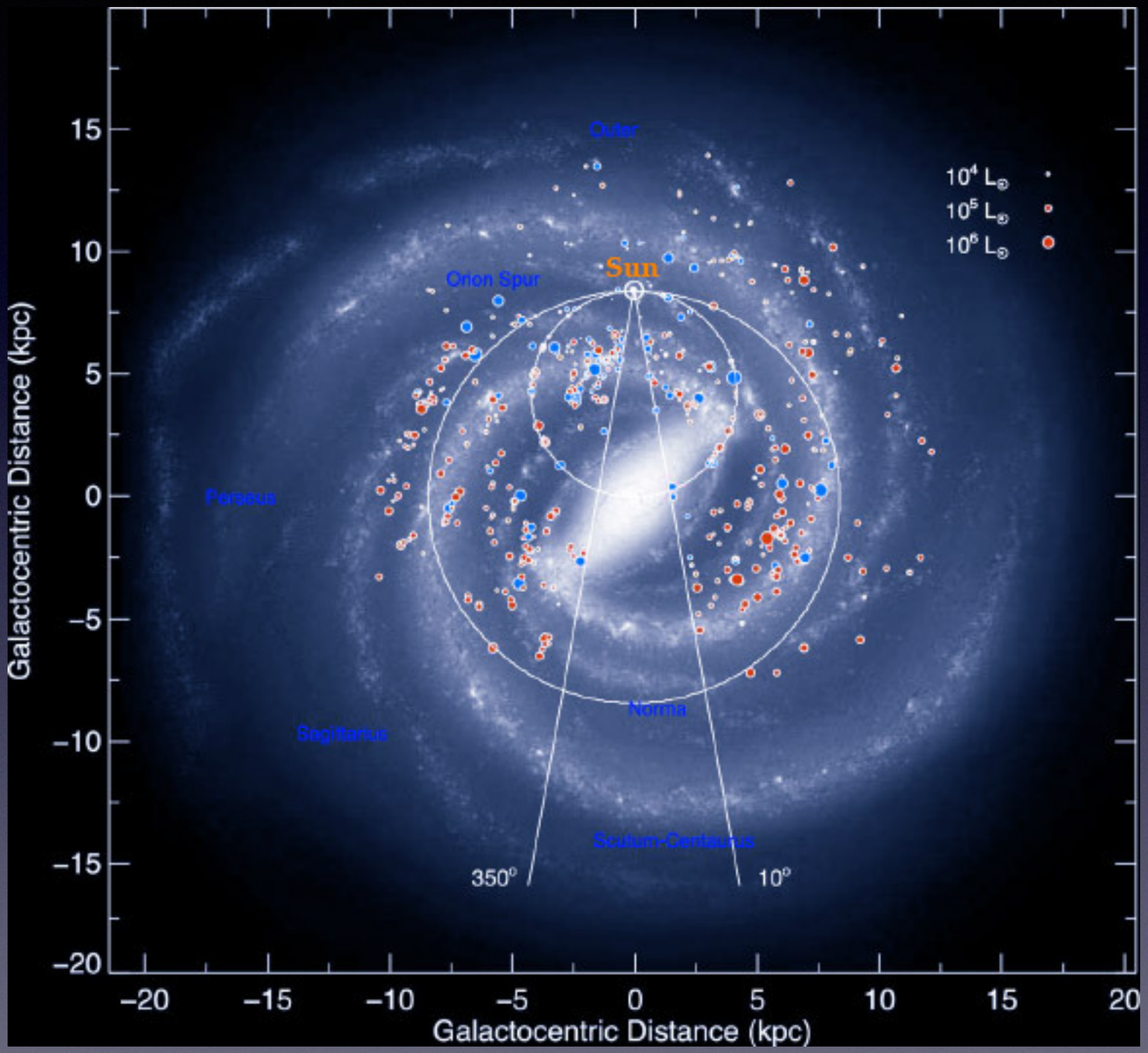

massive young stellar objects (MYSOs) and compact and ultra-compact (UC) H ii regions.

Urquhart etal 2013

History: COBE DIRBE measurements and bar of MW

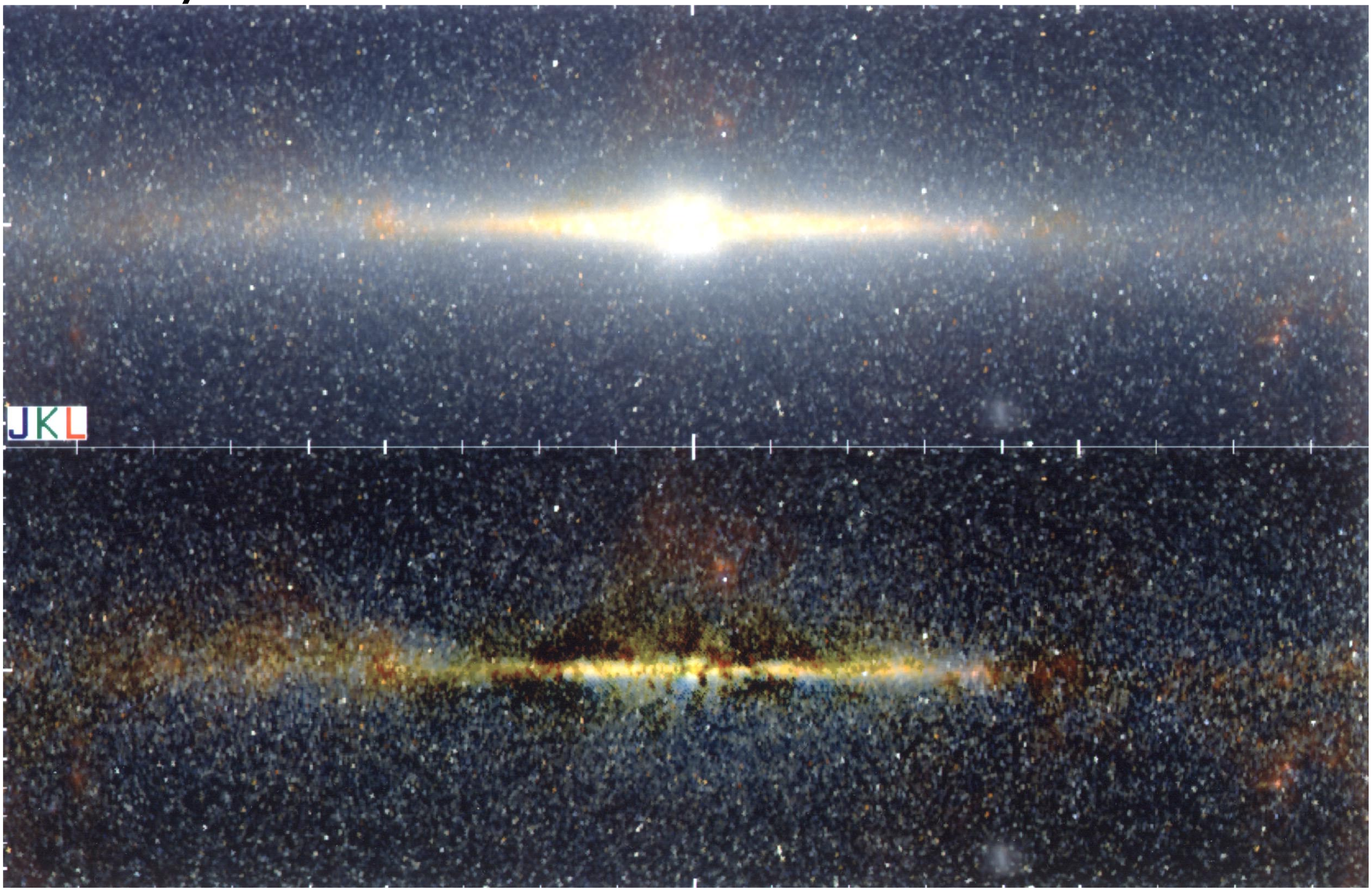

Logarithmic 3-color image of MW. Bottom: residual map

Tick marks are 20deg in l and 5 deg in b

Emission Map

Residual Map

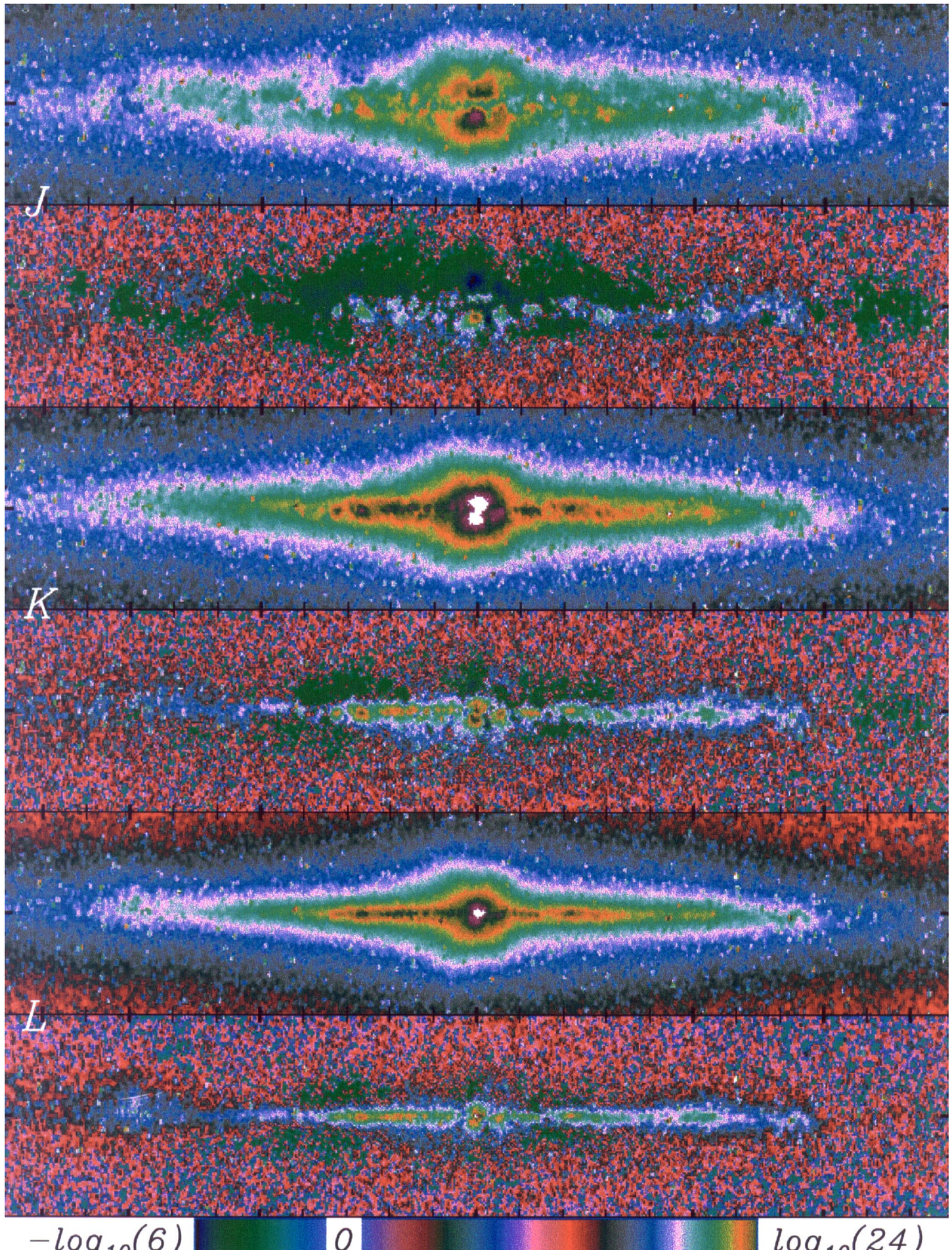

Distribution of Gas

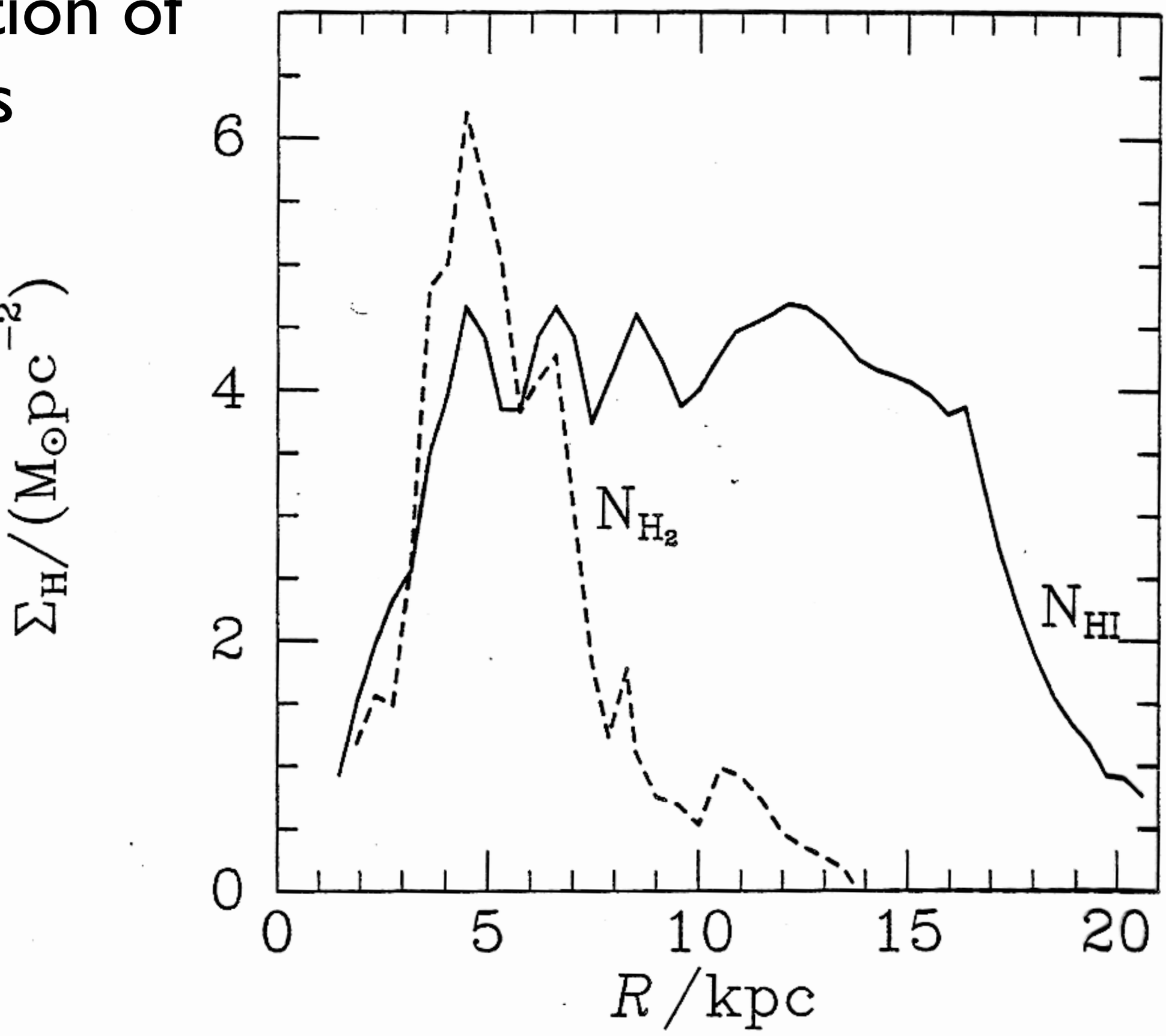

Distribution of Gas

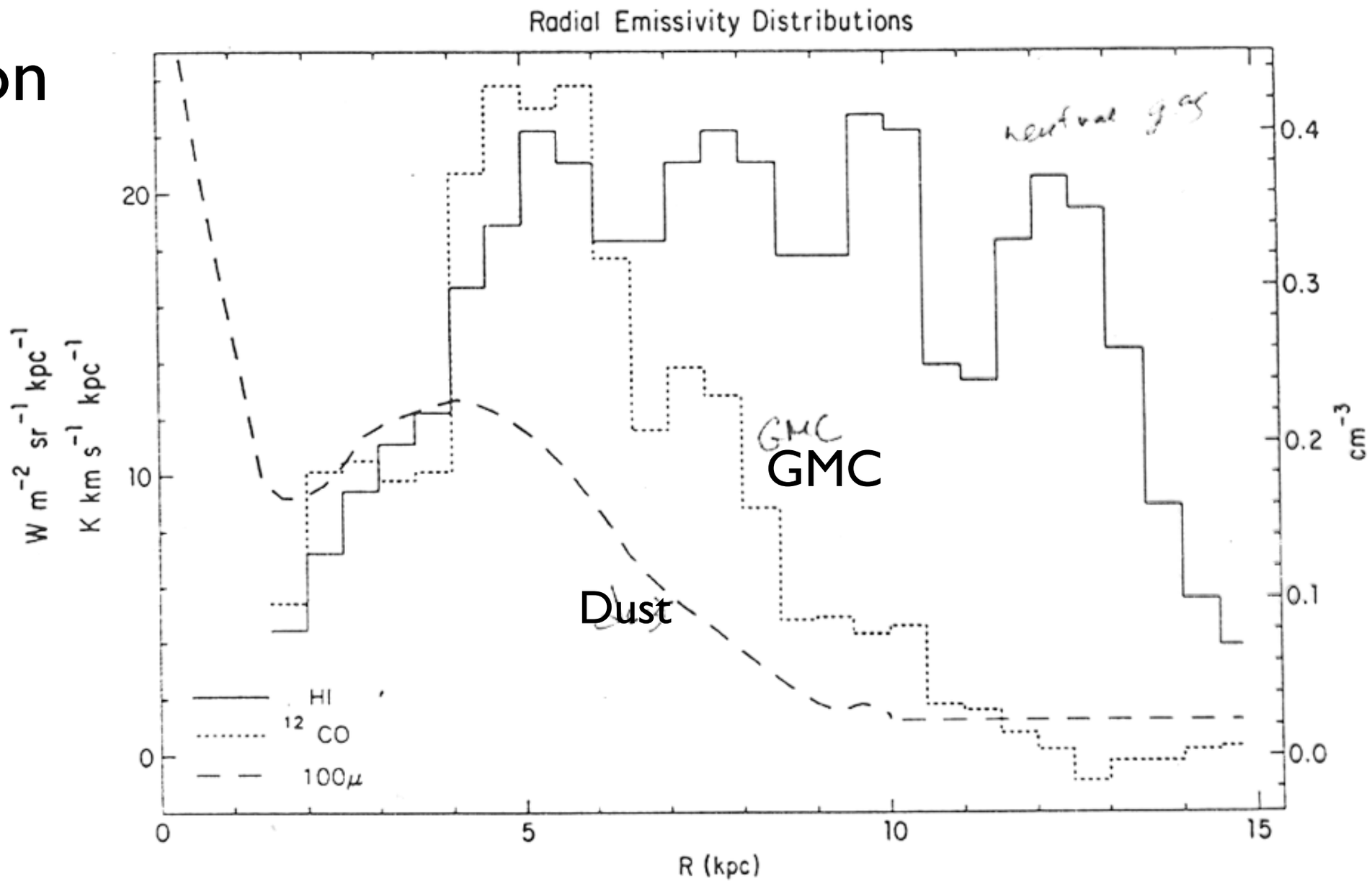

FIGURE 4.2
Radial distributions of HI, CO, and dust. (From Burton 1988.)

much beyond the Sun. Fig. 4.2 compares the GMC distribution with that of HI; the distribution of HII regions would look quite similar to that of the GMCs. The figure also shows the overall distribution of dust, as deduced from the 100 μm IRAS survey.

Height of gas layer

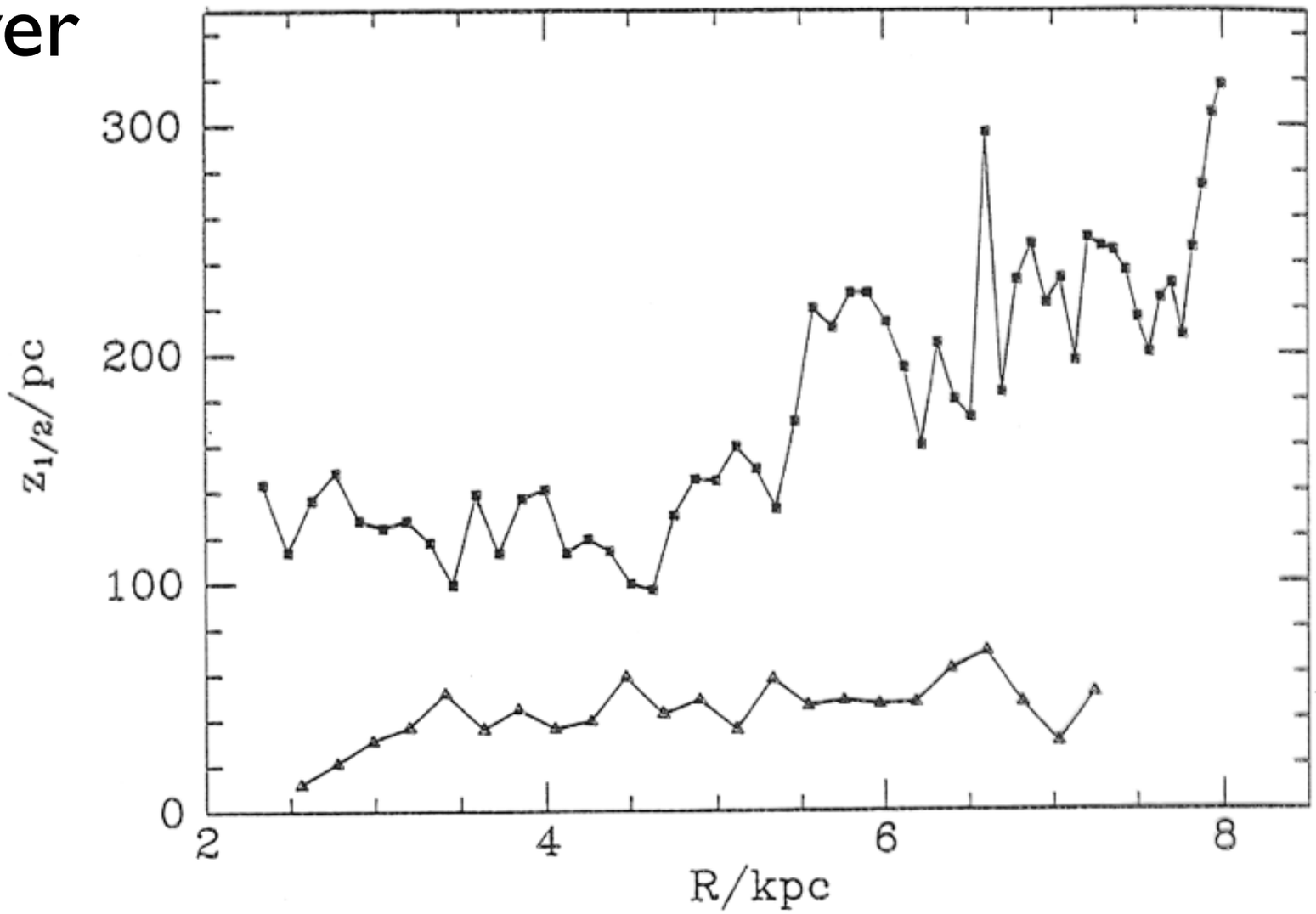

Figure 9.23 The half-height at half-intensity of the HI (squares) and CO (triangles) layers. Open symbols are for $l > 0$ and filled symbols are for $l < 0$. [After Malhotra (1994) and Malhotra (1995) from data kindly provided by S. Malhotra]

Figure 9.23 shows the half-thicknesses at half-intensity $z_{1/2}$ of the HI and CO layers. The thickness of the CO layer is seen to increase slowly with R from $\sim 35\,\mathrm{pc}$ at $R = 3\,\mathrm{kpc}$ to $\sim 70\,\mathrm{pc}$ at $R = R_0$. The HI layer is about three times as thick at a given radius. Thus in the middle disk, the ISM

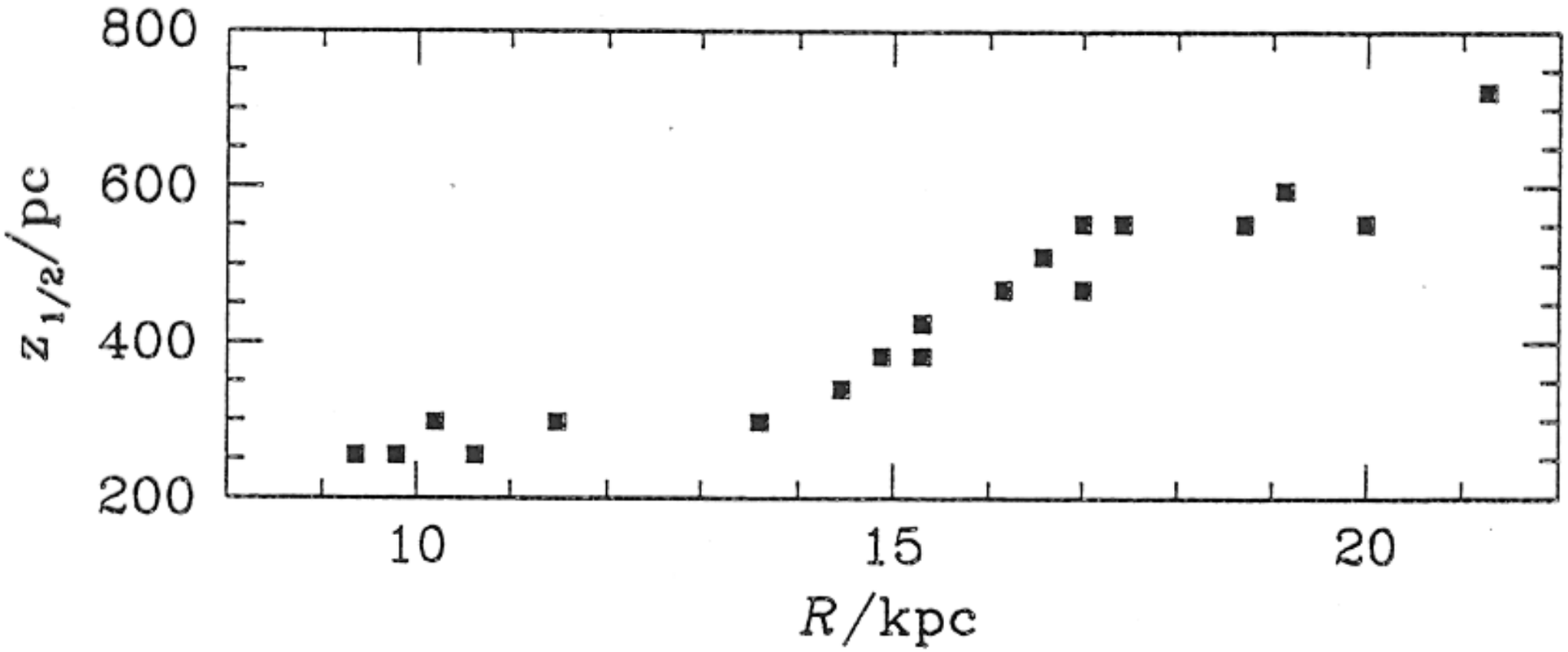

Figure 9.26 The circular-speed curve (top) and the half-thickness at half intensity (below) of the HI layer as determined by Merrifield (1992) using only the 21-cm data of Weaver & Williams (1973,1974) and Kerr *et al.* (1986).

THE ASTROPHYSICAL JOURNAL, 492:495–510, 1998 January 10

A *COBE* MODEL OF THE GALACTIC BAR AND DISK

H. T. FREUDENREICH[1]

History: COBE DIRBE measurements and bar of MW

A model of the bar and old stellar disk of the Galaxy has been derived from the survey of the Diffuse Infrared Background Experiment (DIRBE) of the *Cosmic Background Explorer* at wavelengths of 1.25, 2.2, 3.5, and 4.9 μm. It agrees very well with the data, except in directions in which the near-infrared optical depth is high. Among the conclusions drawn from the model is that the Sun is located approximately 16.5 pc above the midpoint of the Galactic plane. The disk has an outer edge 4 kpc from the Sun and is warped like the H I layer. It has a central hole roughly the diameter of the inner edge of the 3 kpc molecular cloud ring, and within that hole lies a bright, strong, "early-type" bar, tilted approximately 14° from the Sun–Galactic center line. The model has 47 free parameters. The model is discussed

Meanwhile, radio astronomy had been accumulating evidence that the inner part of the Galaxy is less neatly arranged. The radial velocities of gas in the inner few kiloparsecs was found to be inconsistent with travel in circular orbits. In some directions, the velocity is so great that the gas was proposed to lie in an "expanding 3 kpc arm" (Oort, Kerr, & Westerhout 1958) between us and the center; in general, its motion seemed predominantly outward, as if the gas were being driven by titanic explosions near the Galactic center (Burbridge & Hoyle 1963), but this notion lost favor as the improbably vast energy and driven mass required of such explosions came to be better understood (Sanders & Prendergast 1974).

Early interpretation of HI gas motions: expanding 3kpc arm

An alternative explanation is that the gas is moving in noncircular orbits because the potential in which it lies is asymmetric, perhaps because of a bar, as de Vaucouleurs (1964) suggested. Others came to a similar conclusion,

alternative: elliptical motions due to a bar

Model: fitting observational data

The model consists of exponential thin stellar disk, a bar, exponential disk of diffuse dust. Both the thick stellar disk and stellar halo were not included. They are too faint to affect DIRBE fluxes.

The intensity at frequency v in the direction (l, b) is obtained by integrating the volume emissivity ρ along the line of sight s,

$$I_v(l, b) = \delta_v + \int_{(l,b)} ds(\rho_v^{\text{disk}} + \rho_v^{\text{dust}} + \rho_v^{\text{bar}})e^{-\tau_v(s)}$$

The constant δ_v is included to account for possible extragalactic background light and residual zodiacal light

The modeled disk is exponential in R, outer truncated in R, inner truncated in R, sech^2 in Z, and warped. The model does not force the truncations and warping but allows them to occur if the data so dictate.

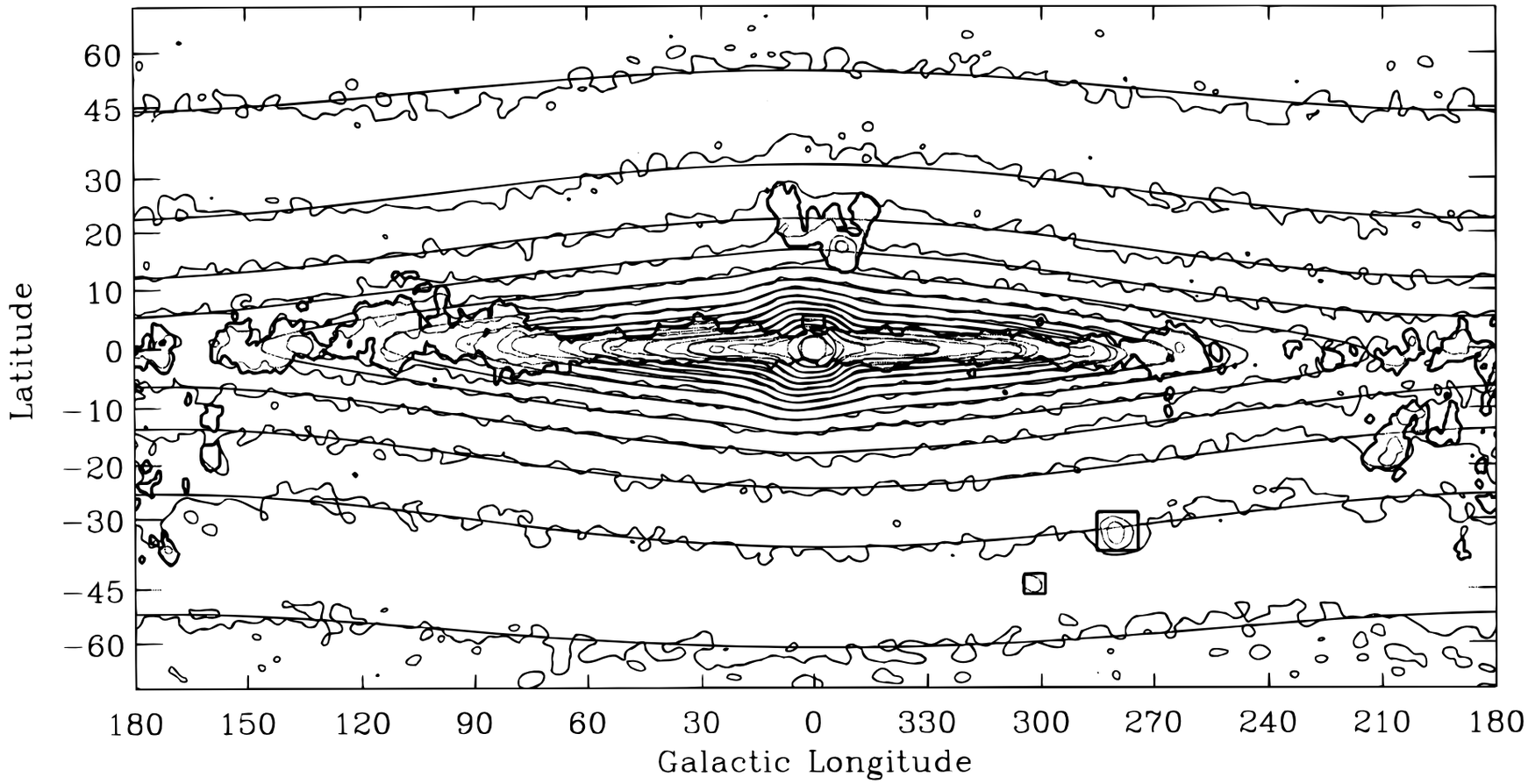

FIG. 3.—*L*-band (3.5 μm) DIRBE and model S (*smooth isophotes*) surface brightness over the full sky. The area within the dark contour was excluded when the model was fitted to the data. The surface brightness due to point sources, as calculated by the model, was added to both. The contour levels are 0.09, 0.13, 0.18, 0.26, 0.52, 0.73, 1.04, 1.47, 2.08, 2.94, 4.17, 5.90, and 8.36 MJy sr^{-1}.

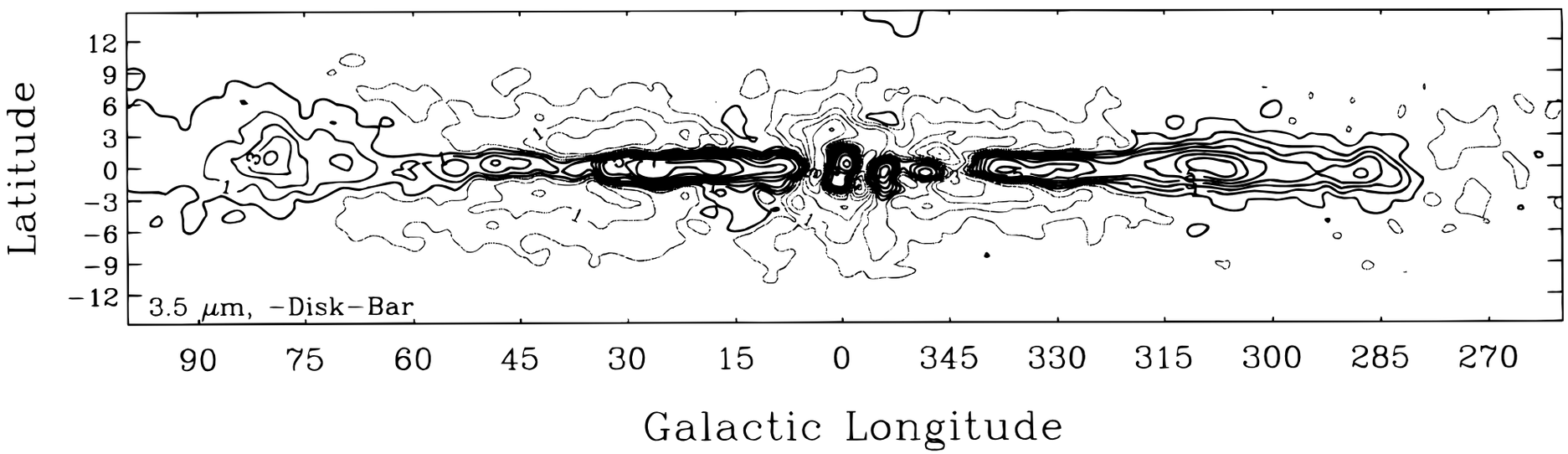

FIG. 8.—*L*-band (3.5 μm) map after the modeled disk and bar are subtracted. The minimal mask was used in fitting the model. The gray contours represent $I_\nu < 0$. Contour levels are numbered hexadecimally, starting at 0. The contour levels are $\pm$ 0.06, 0.21, 0.40, 0.64, 0.94, 1.33, 1.82, 2.43, and 3.21 MJy sr^{-1}.

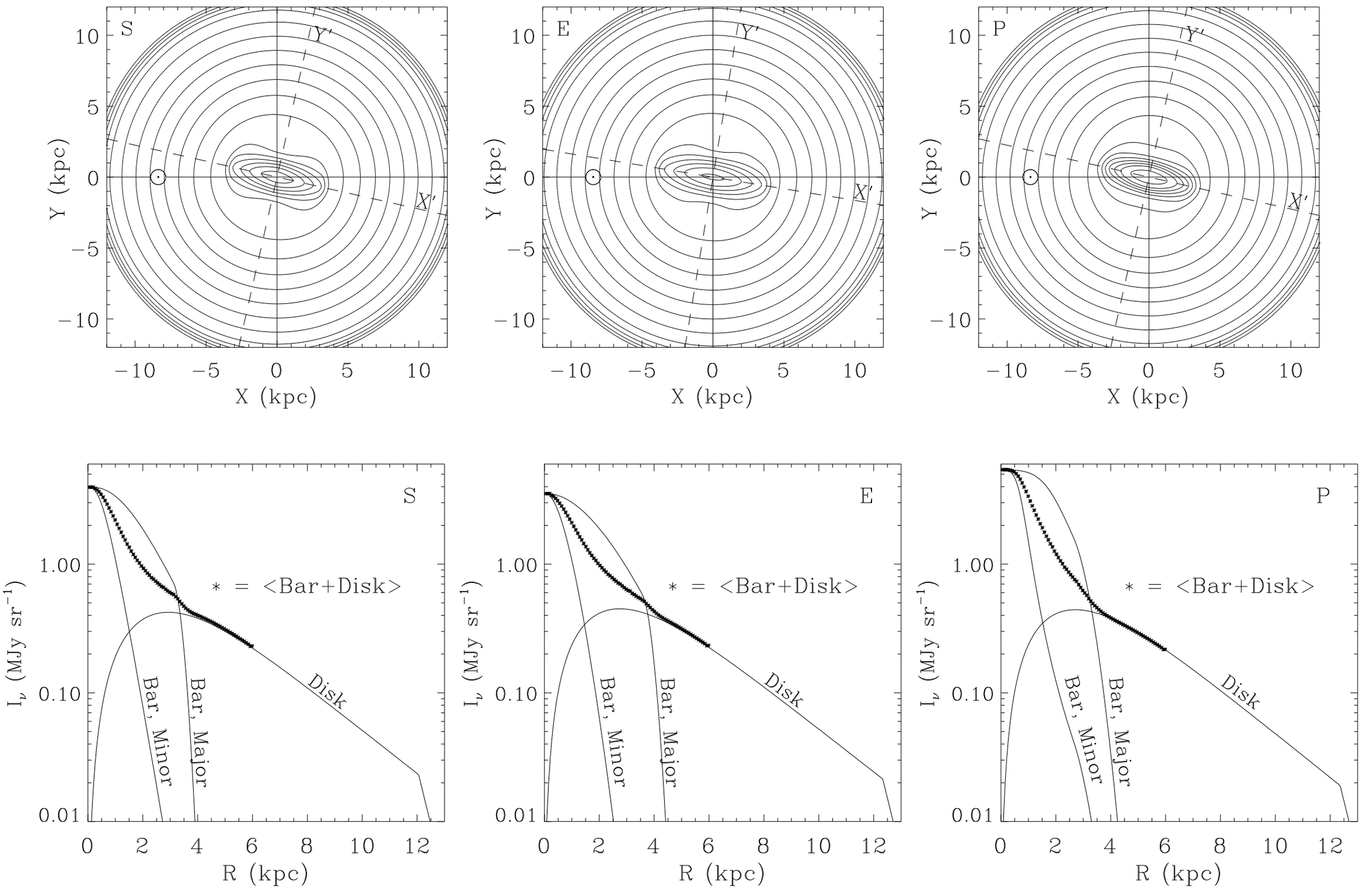

FIG. 14.—*Top*: Log of the face-on surface brightness from models S, E, and P. Our position is marked by the solar symbol. *Bottom*: *L*-band profiles taken along the major and minor axes of the bar. The asterisks denote an average of the bar plus the disk over the azimuth.

Star Counts: SDSS results

THE ASTROPHYSICAL JOURNAL, 553:184–197, 2001 May 20

STELLAR POPULATION STUDIES WITH THE SDSS. I. THE VERTICAL DISTRIBUTION OF STARS IN THE MILKY WAY[1]

BING CHEN,[2] CHRIS STOUGHTON,[3] J. ALLYN SMITH,[4] ALAN UOMOTO,[2] JEFFREY R. PIER,[5] BRIAN YANNY,[3] ŽELJKO IVEZIĆ,[6] DONALD G. YORK,[7] JOHN E. ANDERSON,[3] JAMES ANNIS,[3] JON BRINKMANN,[8] ISTVÁN CSABAI,[2,9] MASATAKA FUKUGITA,[10] ROBERT HINDSLEY,[11] ROBERT LUPTON,[6] AND JEFFREY A. MUNN[5]
(FOR THE SDSS COLLABORATION)

We present star count data from the Sloan Digital Sky Survey for 5.8×10^5 stars brighter than $g' = 21$ mag over 279 deg^2 in two samples north and south of the Galactic plane. Using these high-latitude ($49° < |b| < 64°$) star counts we determine the Sun's distance from the Galactic midplane to be 27 ± 4 pc and the scale height of the old thin disk to be 330 ± 3 pc. Because of the photometric accuracy and large area sky coverage of these data, the color-magnitude diagram clearly reveals a significant thick-disk population distinct in color from a Galactic halo population. The position of the thick-disk turnoff is at $g' - r' \sim 0.33$. Several questions about the existence of the thick disk and its origin are addressed through a set of model fits to the star count data. Our best-fit model gives a thick-disk scale height between 580 and 750 pc, below the original proposal of Gilmore and Reid, and the corresponding space number density normalization is 13%–6.5% of the thin disk. The conclusions reached in this paper favor a scenario in which the thick disk formed through the heating of a preexisting thin disk, with the heating mechanism being the merging of a satellite galaxy.

The density law for the Galactic halo population is also investigated. We find that the data support a flattened halo with $c/a \sim 0.55 \pm 0.06$ and a relatively flat power-law index (2.5 ± 0.3). The axis ratio of the visible halo found in this paper is compatible with that of dark halo, suggesting that they have the same shape and dynamical origin.

Kinematics of stars

$\vec{v} = \{v, u, w\}$

Θ, Π, z

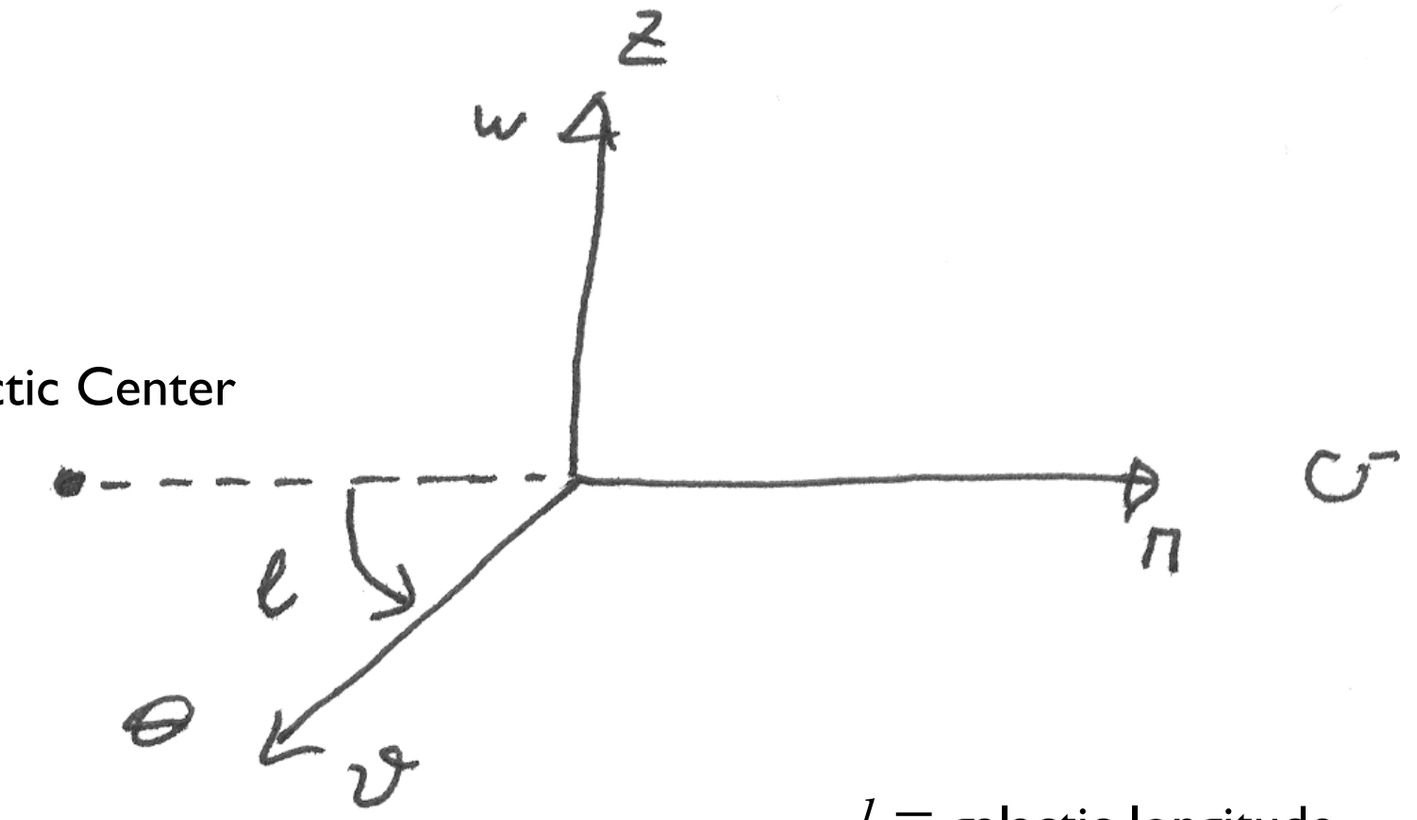

l = galactic longitude

Local standard of rest = object, which moves on a perfect circular orbit

$\vec{V}_{LSR} = \{V_0, 0, 0\}$

Velocity Ellipsoid

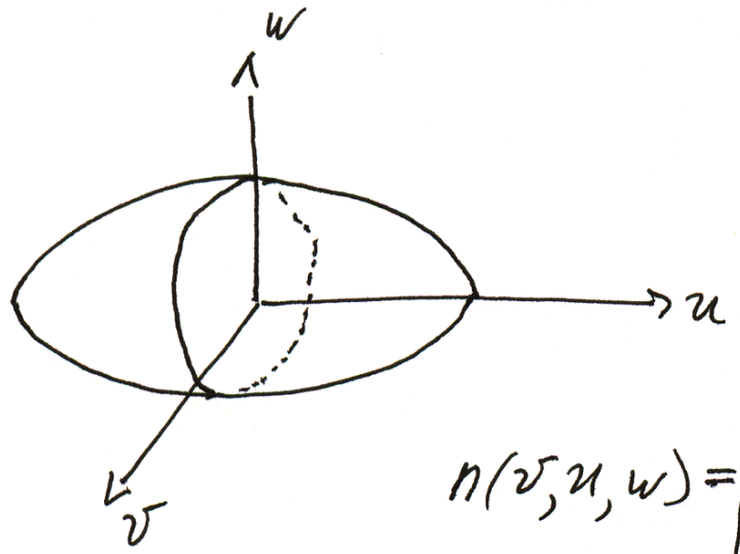

$$n(v,u,w) = \frac{n_0}{\left[8\pi^3 \sigma_u^2 \sigma_v^2 \sigma_w^2\right]^{1/2}} \, e^{-\frac{v^2}{2\sigma_v^2} - \frac{u^2}{2\sigma_u^2} - \frac{w^2}{2\sigma_w^2}}$$

Vortex deviation

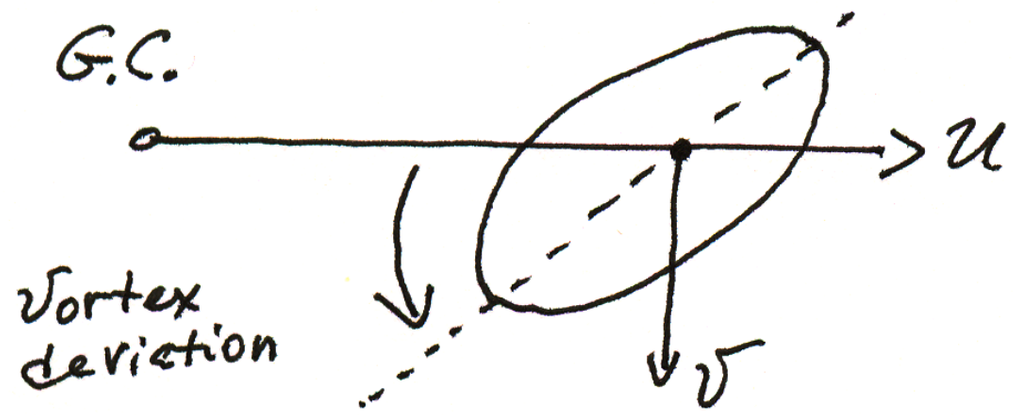

Asymmetric drift

$$V_c^2 \equiv R \frac{\partial \varphi}{\partial R} \qquad V_c - \langle v \rangle = V_a = \text{asymmetric drift}$$

$$V_c^2 - \langle v \rangle^2 = \sigma_u^2 \left[\frac{\sigma_v^2}{\sigma_u^2} - 1 - \frac{\partial \log (n \sigma_u^2)}{\partial \log R} \right] \simeq$$

$$\simeq \sigma_R^2 \left[2 \frac{R}{R_d} - 1.4 \right]$$

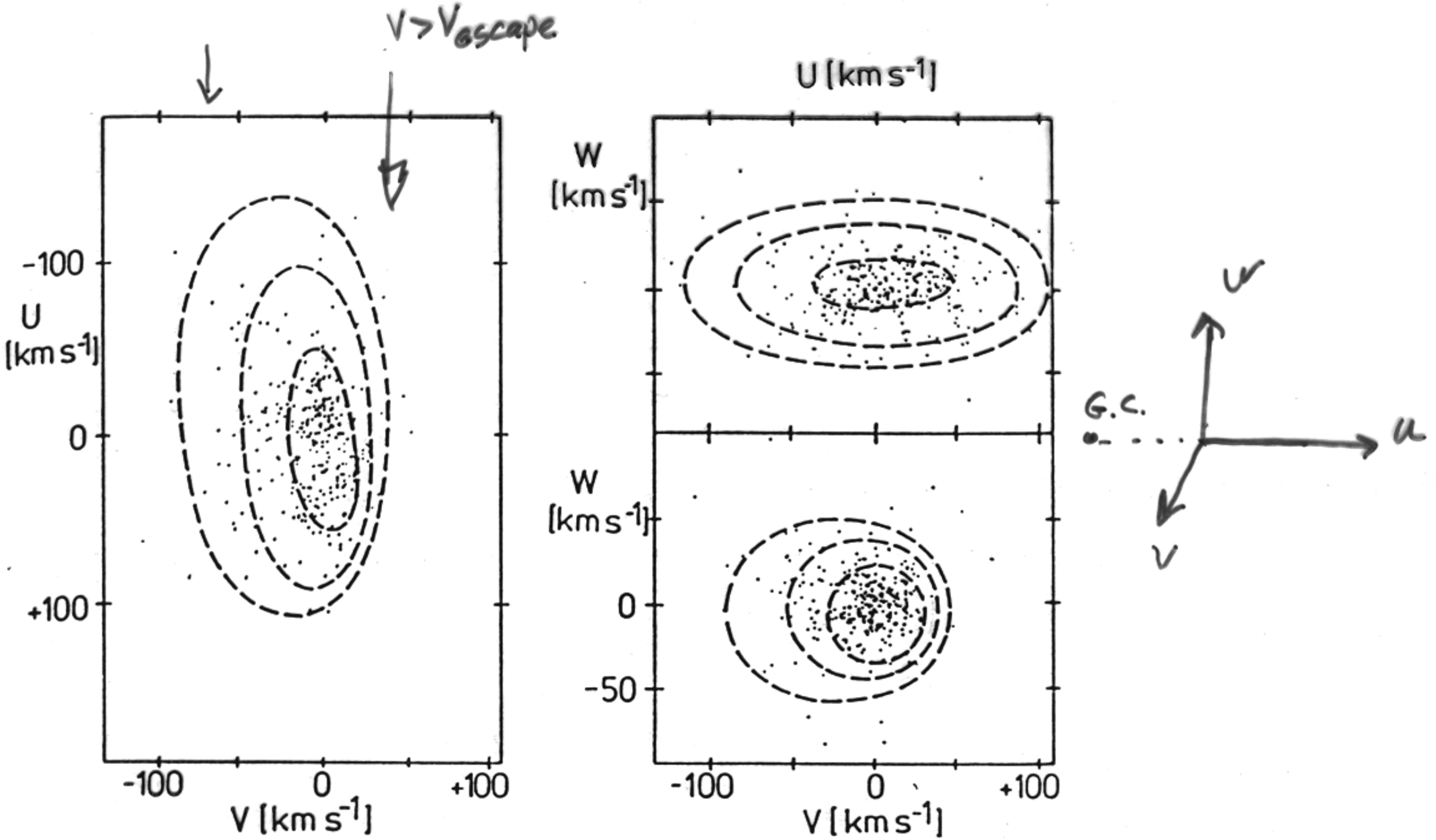

Fig. 3.18. Projections of the velocity distribution of nearby red dwarf stars. Explanation in text

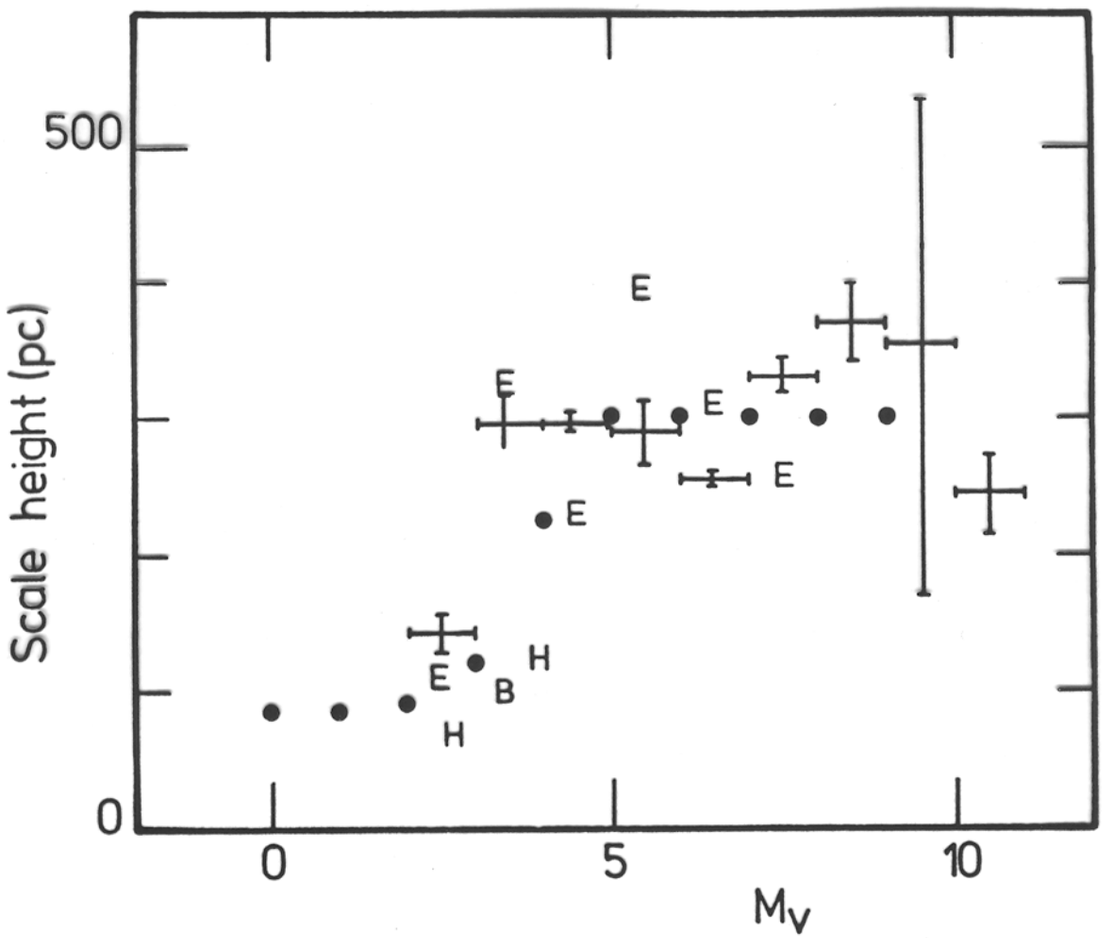

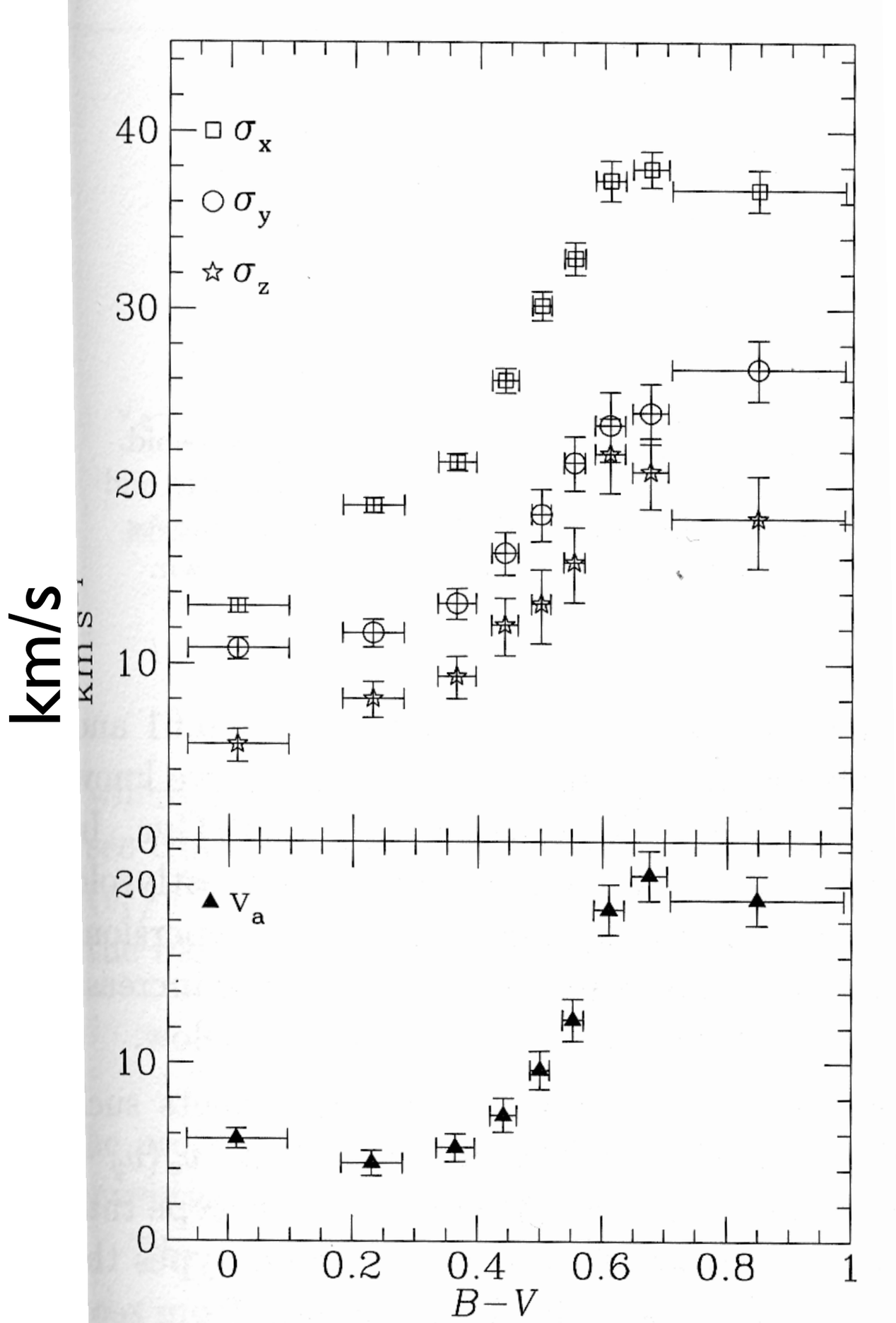

$$V_a = \frac{\langle U^2 \rangle}{80 \pm 5\,\mathrm{km\,s^{-1}}}$$

Galaxy Disks and Disk Galaxies
ASP Conference Series, Vol. 230, 2001
J.G. Funes, S.J., and E.M. Corsini, eds.

The Saturation of Disk Heating in the Solar Neighborhood and Evidence for a Merger 9 Gyr Ago

A. C. Quillen and D. R. Garnett

Steward Observatory, University of Arizona, Tucson, AZ, USA

Abstract. We re-examine the age-velocity dispersion relation in the solar neighborhood using improved stellar age estimates which are based on Hipparcos parallaxes and recent stellar evolution calculations. The resulting relation shows that the Milky Way stellar disk was relatively quiescent, suffering little heating or dispersion increase between 3 and 9 Gyr. However, at an age of 9 Gyr there is an abrupt increase in the stellar velocity dispersions. To explain the abrupt increase (by almost a factor of 2) in dispersions we propose that the Milky Way suffered a minor merger 9 Gyr ago that created the thick disk. The quiescent phase is consistent with inefficient heating caused by scattering from tightly wound transient spiral structure.

We have used the sample of 189 nearby, slightly-evolved F and G dwarf stars from Edvardsson et al. (1993) to re-derive the age-velocity dispersion relation in the solar neighborhood (Quillen & Garnett 2001). These stars have accurate metallicities, distances, and kinematic data, so it is possible to derive accurate stellar ages. The sample is generally considered to be kinematically unbiased (Freeman 1991). For these stars, we have obtained parallaxes and proper motions from the HIPPARCOS catalog and new, accurate ages from Ng & Bertelli (1998). Accurate ages are important to avoid smoothing over fine structure

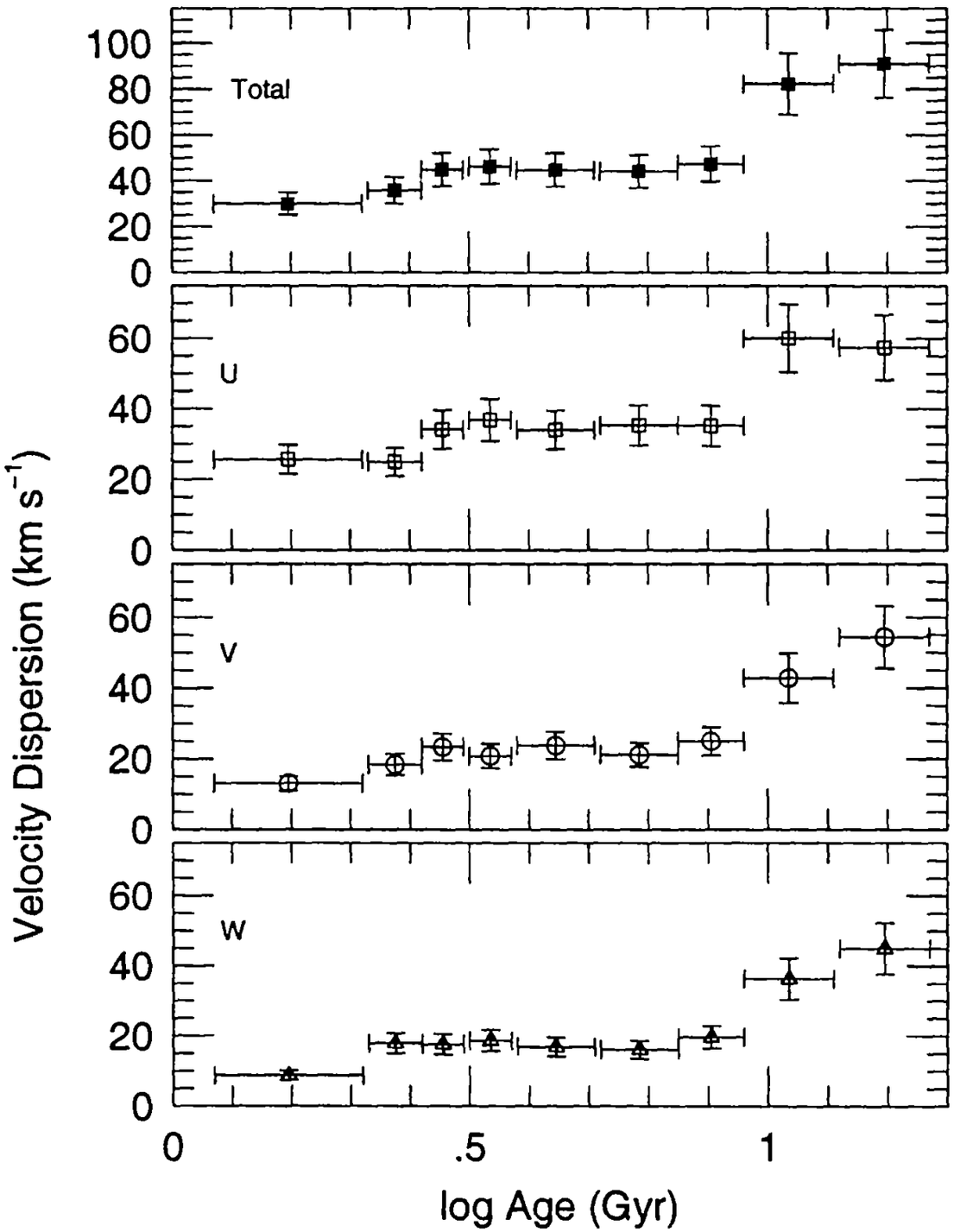

Figure 1. Velocity dispersion vs. log age for stars from Edvardsson et al. (1993). The vertical error bars represent statistical uncertainties; horizontal error bars represent the width of each age bin.

Disk:

- early-type stars have smaller rms velocities and their velocity ellipsoid is not pointed to the galactic center.
- late-type stars have larger rms velocities and almost no vertex deviation
- typical ratio of velocities $\sigma_R : \sigma_\varphi : \sigma_z = 1 : 0.65 : 0.5$
- typical values: 30:20:15 km/s
- important: $\sigma_R \neq \sigma_z$
- velocity dispersion declines with the distance to the galactic center

Halo and thick disk kinematics

THE ASTRONOMICAL JOURNAL, 119:2843–2865, 2000 June

Chiba & Beers

Data:

1203 stars with proper motions, metallicities [Fe/H] < -0.6, distances, radial velocities. Galactocentric distances R in the range 7-10 kpc. Distances from the Sun D< 4 kpc.

stars with -0.7 <[Fe/H] < -0.6 and |Z|<1kpc are mostly the thick disk stars

TABLE 1

MEAN VELOCITIES AND VELOCITY DISPERSIONS OF THE SELECTED SAMPLE

[Fe/H] (dex)	N	$\langle U \rangle$ (km s^{-1})	$\langle V \rangle$ (km s^{-1})	$\langle W \rangle$ (km s^{-1})	σ_U (km s^{-1})	σ_V (km s^{-1})	σ_W (km s^{-1})
			$\lvert Z \rvert < 1$ kpc				
-0.6 to -0.8.....	141	2 ± 4	-30 ± 5	-5 ± 3	50 ± 3	56 ± 3	34 ± 2
-0.8 to -1.0.....	79	7 ± 10	-62 ± 10	1 ± 6	93 ± 7	86 ± 7	50 ± 4
-1.0 to -1.6.....	194	8 ± 9	-122 ± 7	-1 ± 6	122 ± 6	104 ± 5	81 ± 4
-1.6 to -2.2.....	205	23 ± 10	-178 ± 8	-2 ± 6	147 ± 7	115 ± 6	87 ± 4
≤ -2.2	78	17 ± 16	-187 ± 12	-5 ± 11	141 ± 11	106 ± 9	94 ± 8
			$\lvert Z \rvert < 4$ kpc				
-0.6 to -0.8.....	197	4 ± 5	-43 ± 4	-2 ± 3	65 ± 3	62 ± 3	40 ± 2
-0.8 to -1.0.....	97	2 ± 10	-74 ± 9	3 ± 5	94 ± 7	84 ± 6	49 ± 4
-1.0 to -1.6.....	280	5 ± 8	-137 ± 6	-4 ± 5	129 ± 5	108 ± 5	81 ± 3
-1.6 to -2.2.....	327	8 ± 8	-189 ± 7	-1 ± 5	154 ± 6	121 ± 5	86 ± 3
≤ -2.2	141	13 ± 13	-200 ± 10	-5 ± 9	151 ± 9	121 ± 7	103 ± 6

U = radial velocities (cylindrical coords)
V = tangential velocities
W= vertical velocities

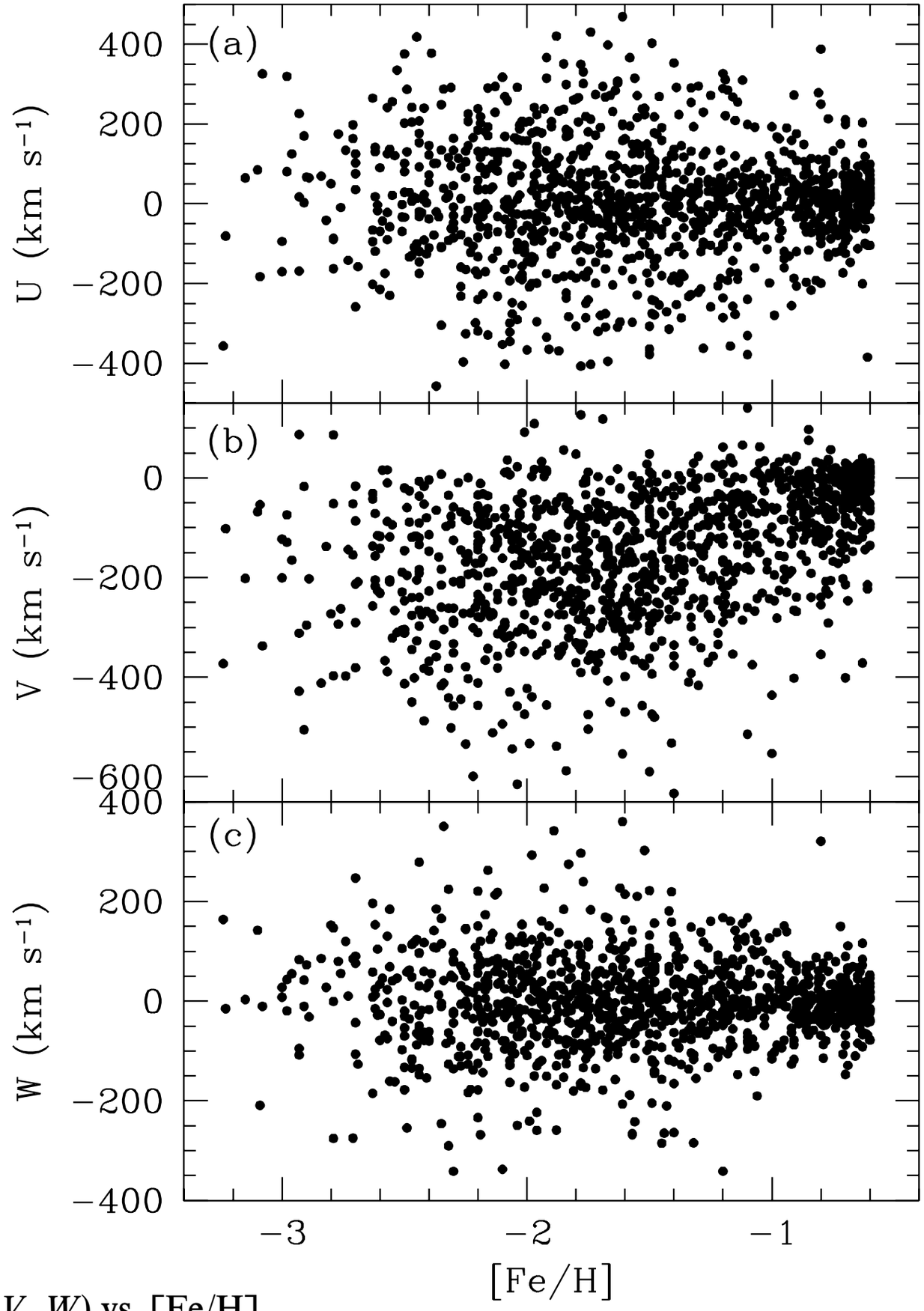

FIG. 1.—Distribution of the velocity components (U, V, W) vs. [Fe/H] for the 1203 stars with available proper motions.

Velocity dispersion as function of metallicity

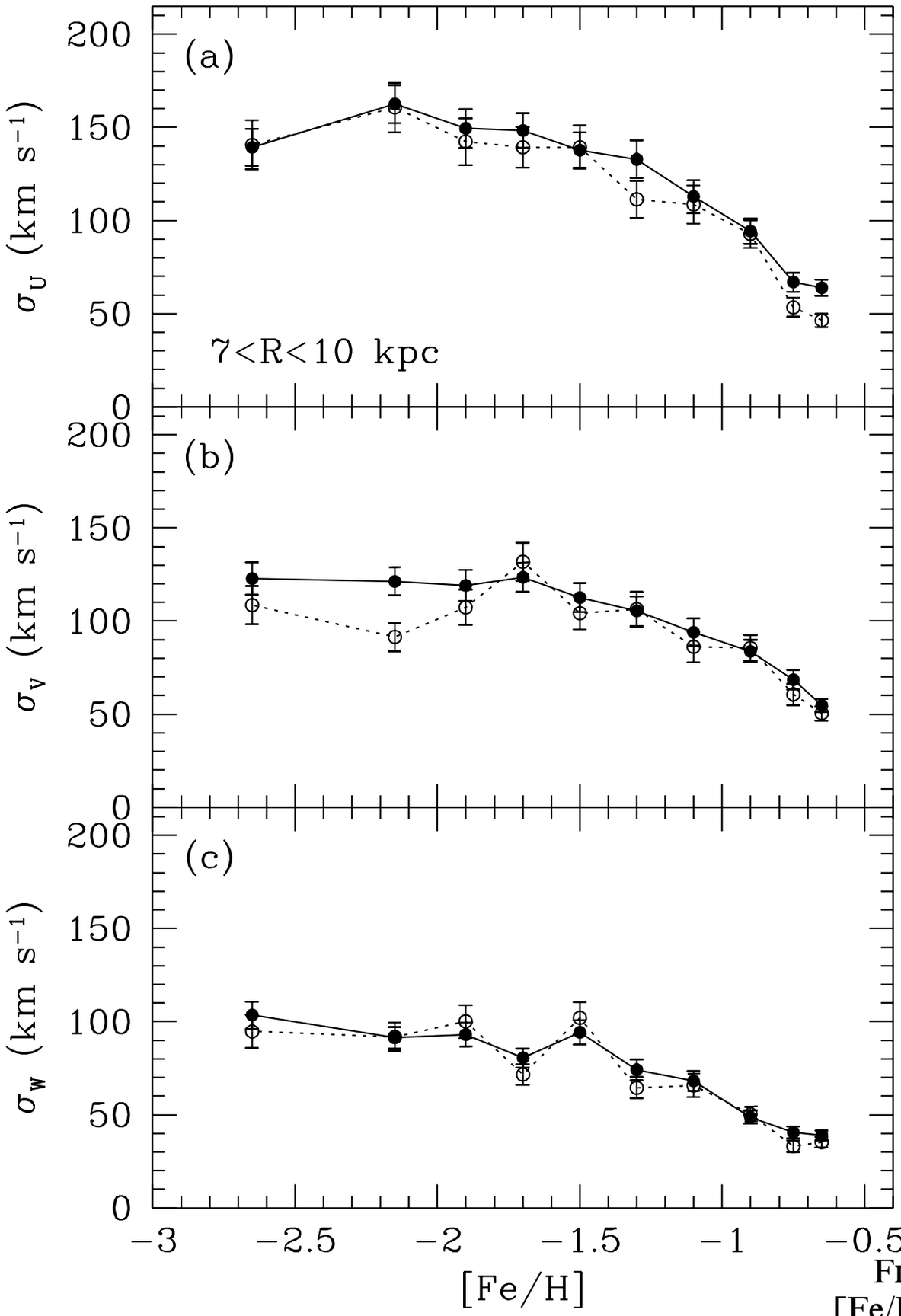

FIG. 2.—Distribution of the velocity dispersions (σ_U, σ_V, σ_W) vs. [Fe/H] for the selected sample with $7 < R < 10$ kpc, $D < 4$ kpc, and $V_{\rm RF} \leq 550$ km s^{-1}. Filled and open circles denote the stars at $|Z| < 1$ kpc and $|Z| < 4$ kpc, respectively.

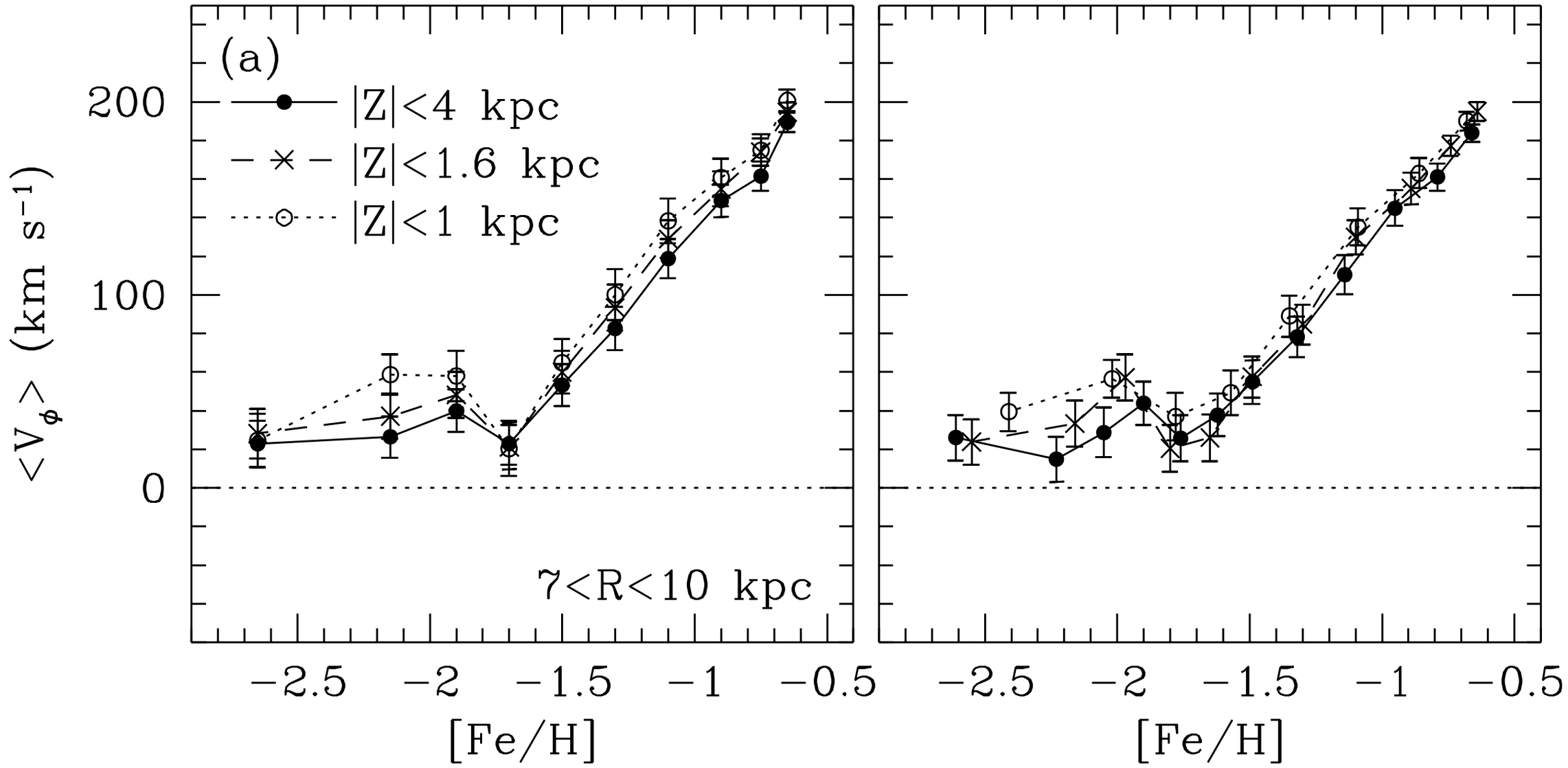

FIG. 3.—Distribution of the mean rotational velocities $\langle V_\varphi \rangle$ vs. [Fe/H] for the selected sample, assuming an LSR rotation velocity of 220 km s^{-1}. Left-hand panels show the results for characteristic abundance ranges, whereas in the right-hand panels, we calculate $\langle V_\varphi \rangle$ by passing a box of width $N = 100$ stars (ordered by metallicity), with an overlap of 20 stars each. (*a*) Based on the full knowledge of proper motions and radial velocities. Filled circles, crosses, and open circles correspond to the stars at $|Z| < 4$ kpc, $|Z| < 1.6$ kpc, and $|Z| < 1$ kpc, respectively. (*b*) Based on the Frenk & White methodology using

Rotational velocity as function of metallicity

Rotational velocity as function of distance to the galactic plane

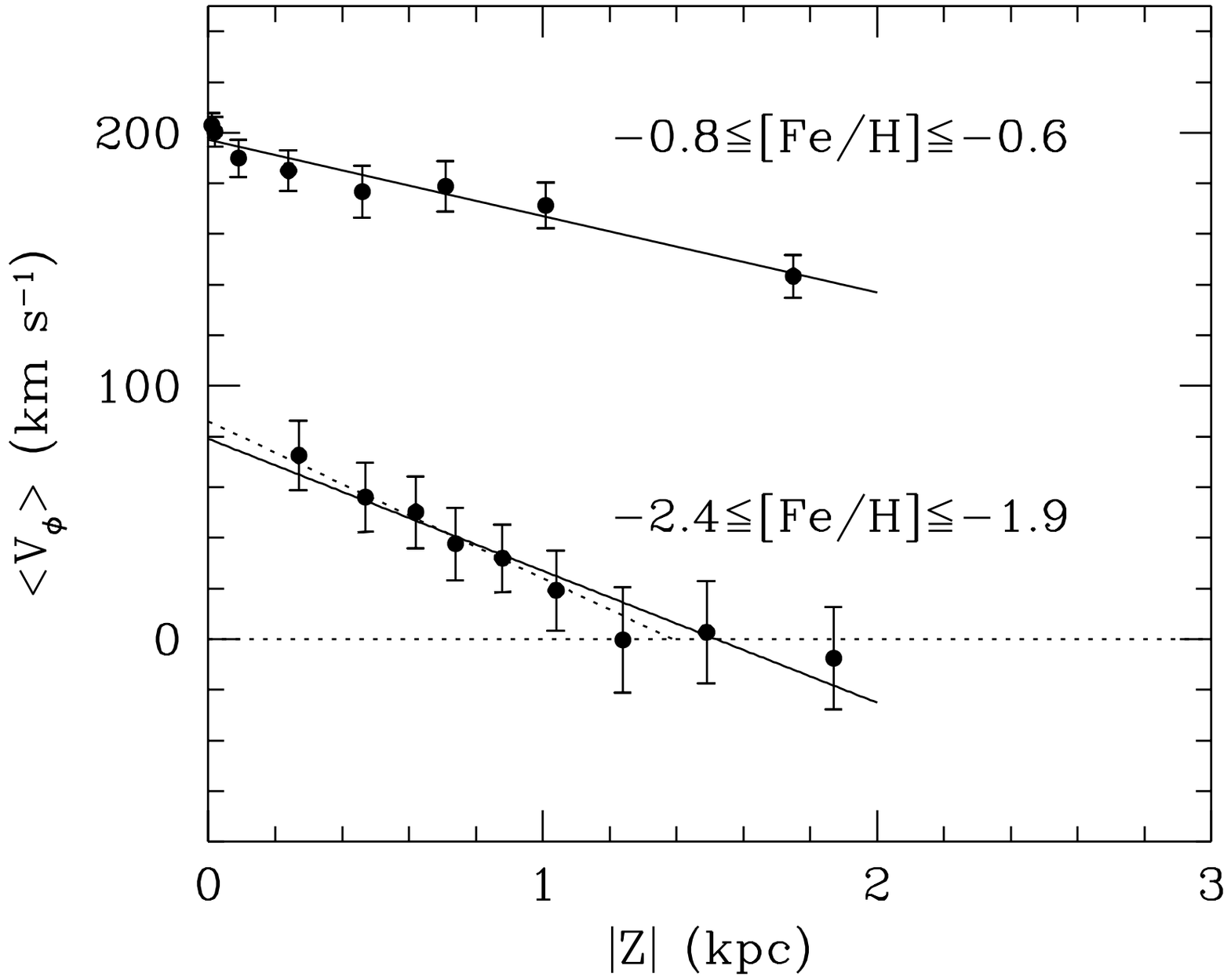

FIG. 4.—Distribution of the mean rotational velocities, $\langle V_\varphi \rangle$, vs. $|Z|$ for stars of the selected sample in the abundance ranges $-2.4 \leq$ [Fe/H] ≤ -1.9 and $-0.8 \leq$ [Fe/H] ≤ -0.6, respectively. The binning in $|Z|$ is made by sweeping a box of 50 stars through the data (ordered by $|Z|$), with an overlap of 30 stars. Solid lines are least-square fits to the data. The dotted line for $-2.4 \leq$ [Fe/H] ≤ -1.9 is the fit obtained after excluding the last point at $|Z| = 1.76$ kpc.

Conclusions:

- Stars with [Fe/H]<-2.2, which likely represent a pure halo, have radially elongated velocity ellipsoid:

$$(\sigma_U, \sigma_V, \sigma_W) = (141 \pm 11,\ 106 \pm 9,\ 94 \pm 8)\ \mathrm{km\ s^{-1}}$$

- They have small prograde rotation $<V_\varphi>$=30-50km/s
- $<V_\varphi>$ decreases with the distance from the plane
- There is NO correlation between orbital eccentricity and [Fe/H]

- Intermediate-abundance stars close to the plane of the disk (thick disk) have large $<V_\varphi>$=200km/s. Their velocity ellipsoid:

$$(\sigma_U,\ \sigma_V,\ \sigma_W) = (46 \pm 4,\ 50 \pm 4,\ 35 \pm 3)\ \mathrm{km\ s^{-1}}$$

Halo: large distances

Assuming isotropic velocities (may not be right), observation give:

At 50kpc σ_{3D} = 190km/s

At 100kpc σ_{3D} = 120km/s

Virial mass of 10^{12}Msun is marginally ok, but it is on a high side.
Isothermal ("constant rotation") halo is rejected

Battaglia et al

Mon. Not. R. Astron. Soc. **364,** 433–442 (2005)

The radial velocity dispersion profile of the Galactic halo: constraining the density profile of the dark halo of the Milky Way

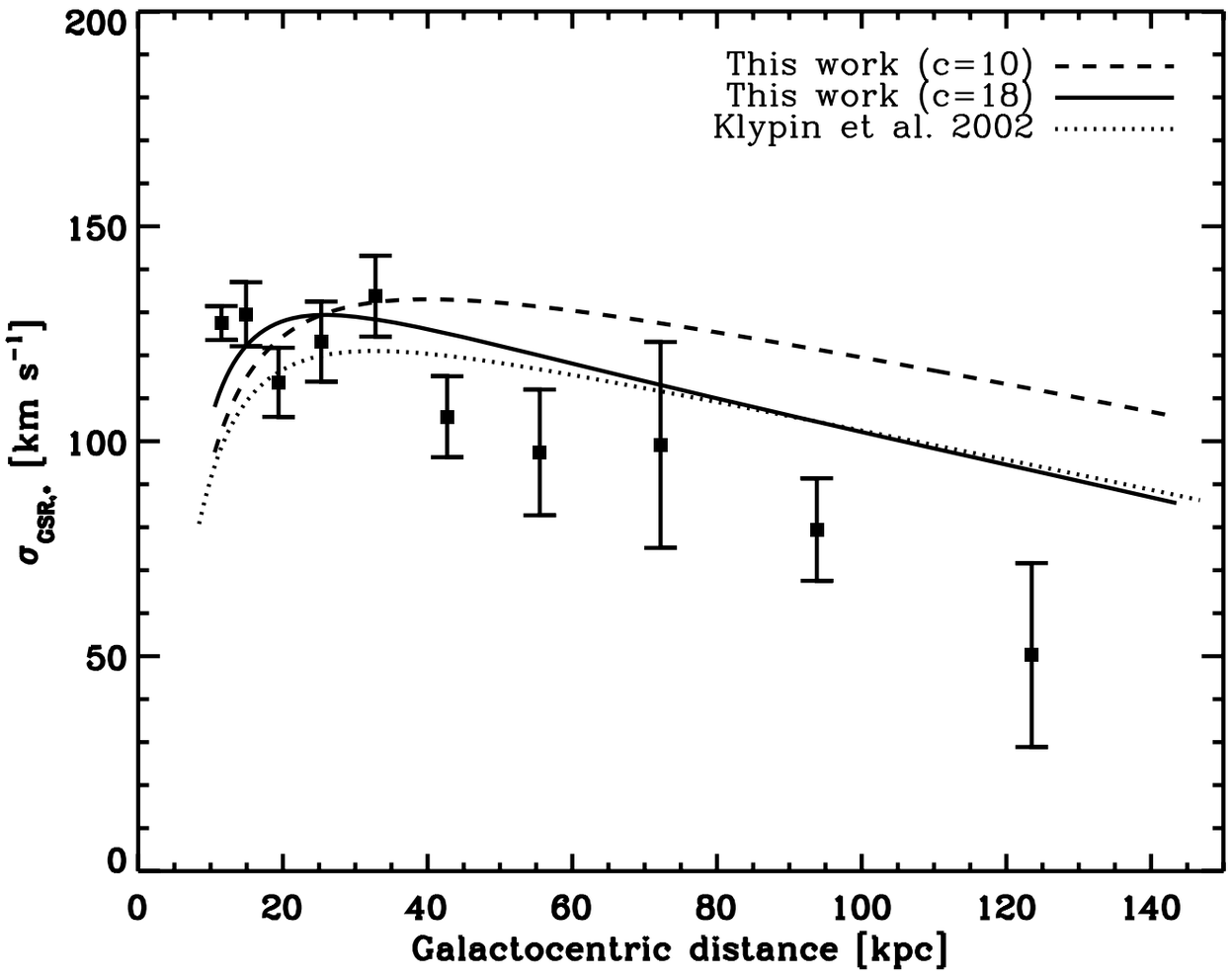

Figure 1. Observed radial velocity dispersion (squares with error bars) overlaid on two of the best-fitting models for the NFW mass distributions (dashed line: $c = 10$; solid line: $c = 18$). The dotted curve corresponds to the Galactocentric radial velocity dispersion profile obtained using the preferred model (B1) of Klypin et al. (2002). This figure replaces the bottom panel of fig. 4 in the original manuscript.

Table 1. Characteristics of the data used in this paper. In all cases, position in the sky, heliocentric distance and line-of-sight velocities are available.

Objects	Number of objects	Source
Globular clusters	44	Harris (1996)
FHB stars	130	Wilhelm et al. (1999), Clewley et al. (2004)
Red halo giants	57	Spaghetti survey
Satellite galaxies	9	Mateo (1998)

$$M(< 60\ \mathrm{kpc}) = 4.0 \pm 0.7 \times 10^{11} M_{\odot}$$

$$M_{vir} = 1.0^{+0.3}_{-0.2} \times 10^{12} M_{\odot}$$

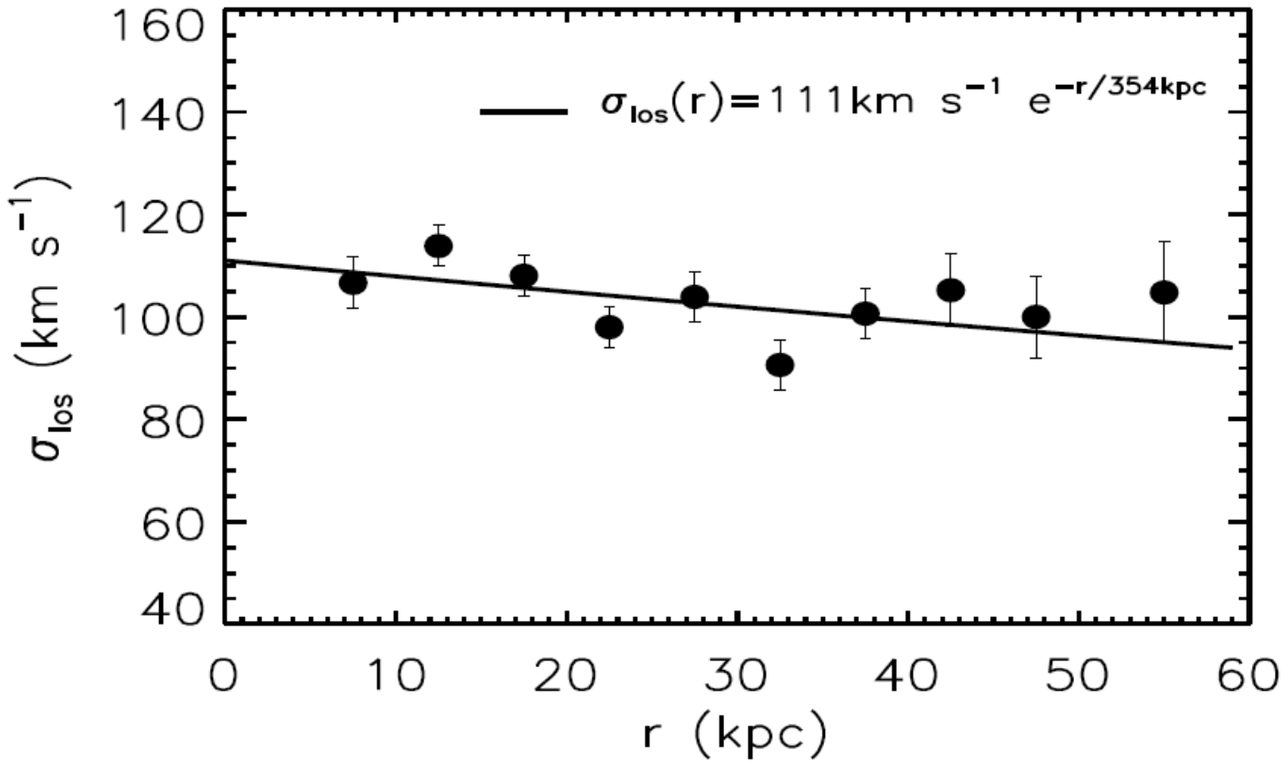

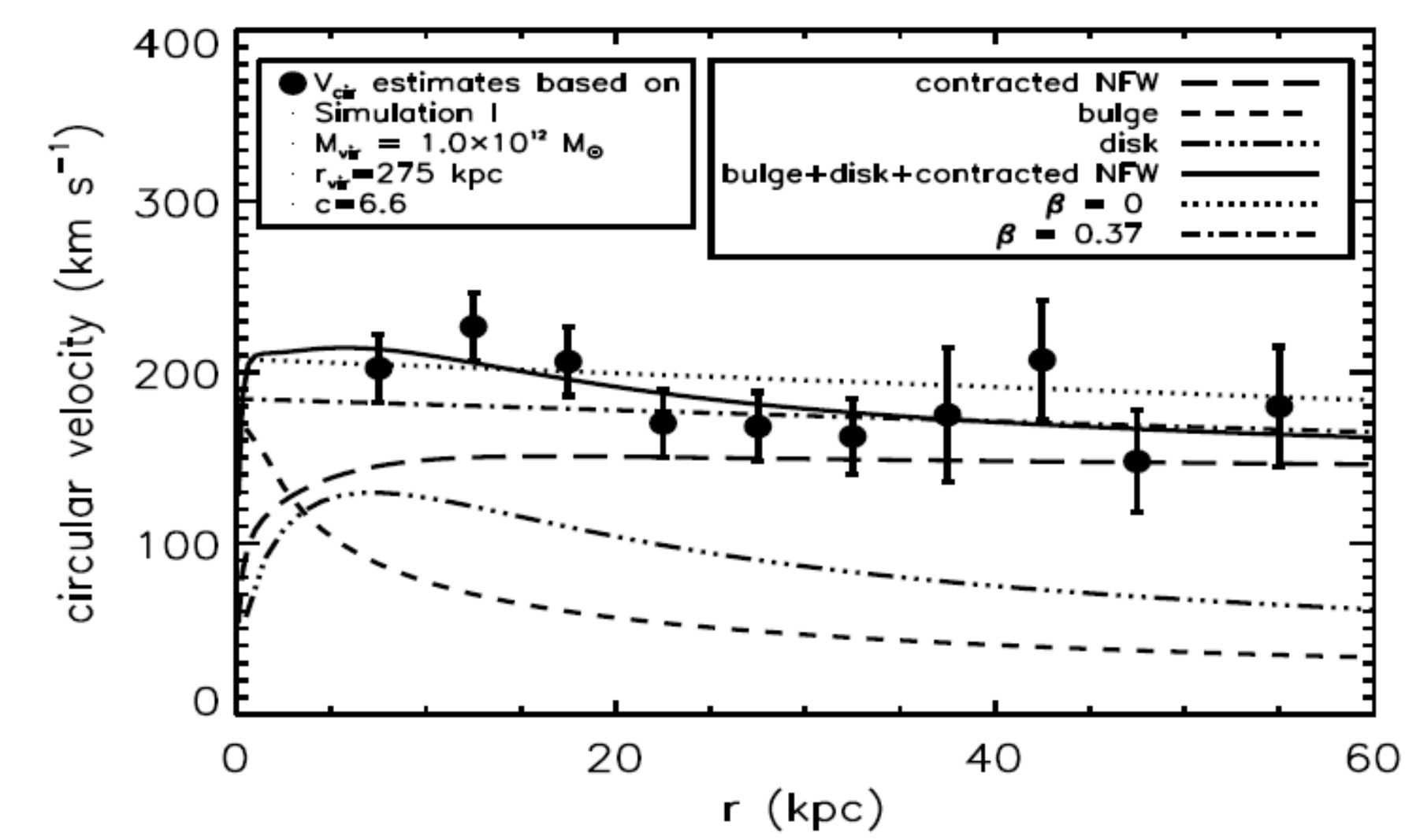

Mass modeling of MW

ΛCDM-BASED MODELS FOR THE MILKY WAY AND M31.

THE ASTROPHYSICAL JOURNAL, 573:597–613, 2002

Circular velocity curve of our Galaxy (symbols).

Different curves show contributions from different mass components.

Dark matter is the dominant component at radii larger than ~15 kpc while normal matter dominates in the central region.

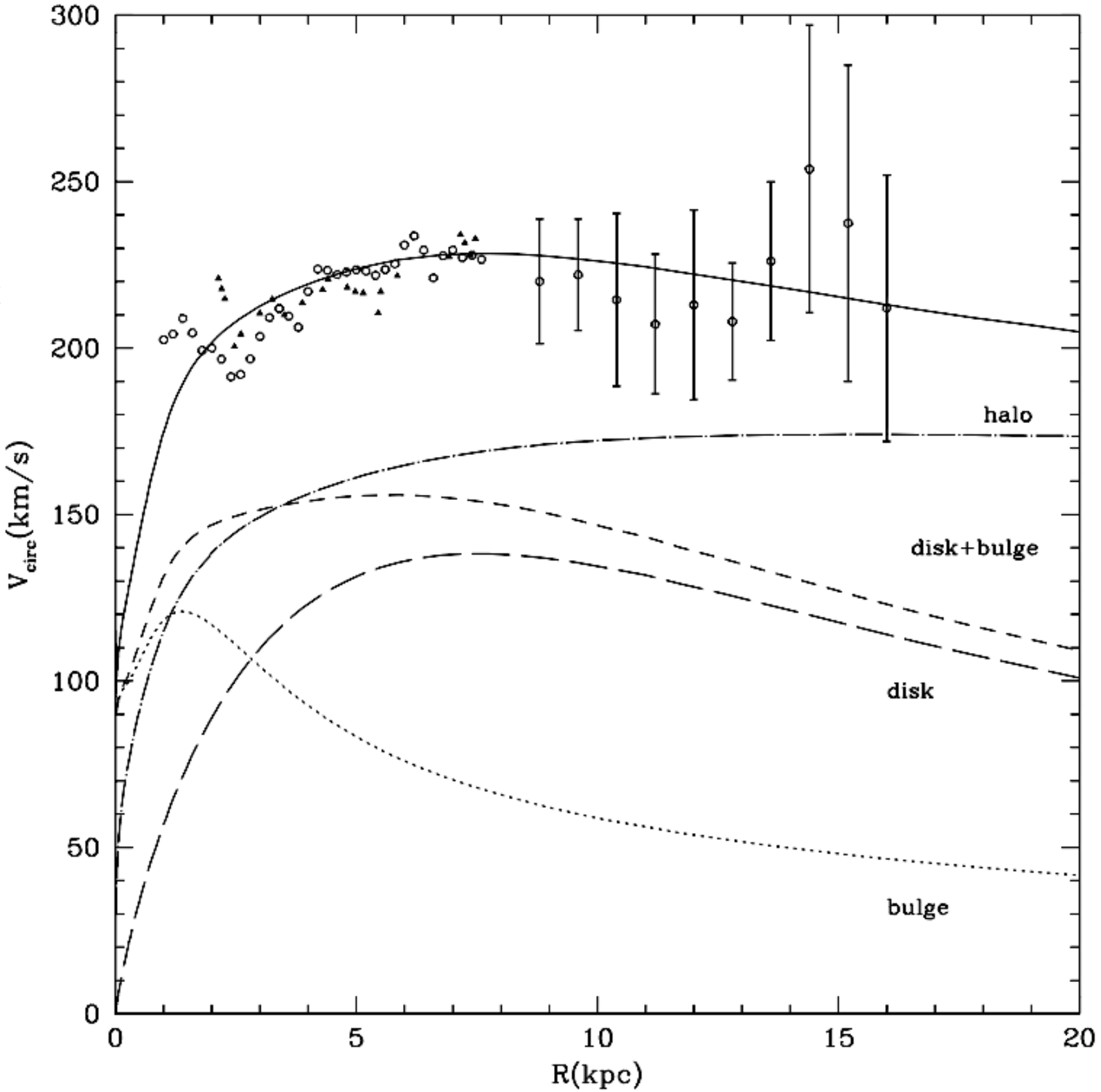

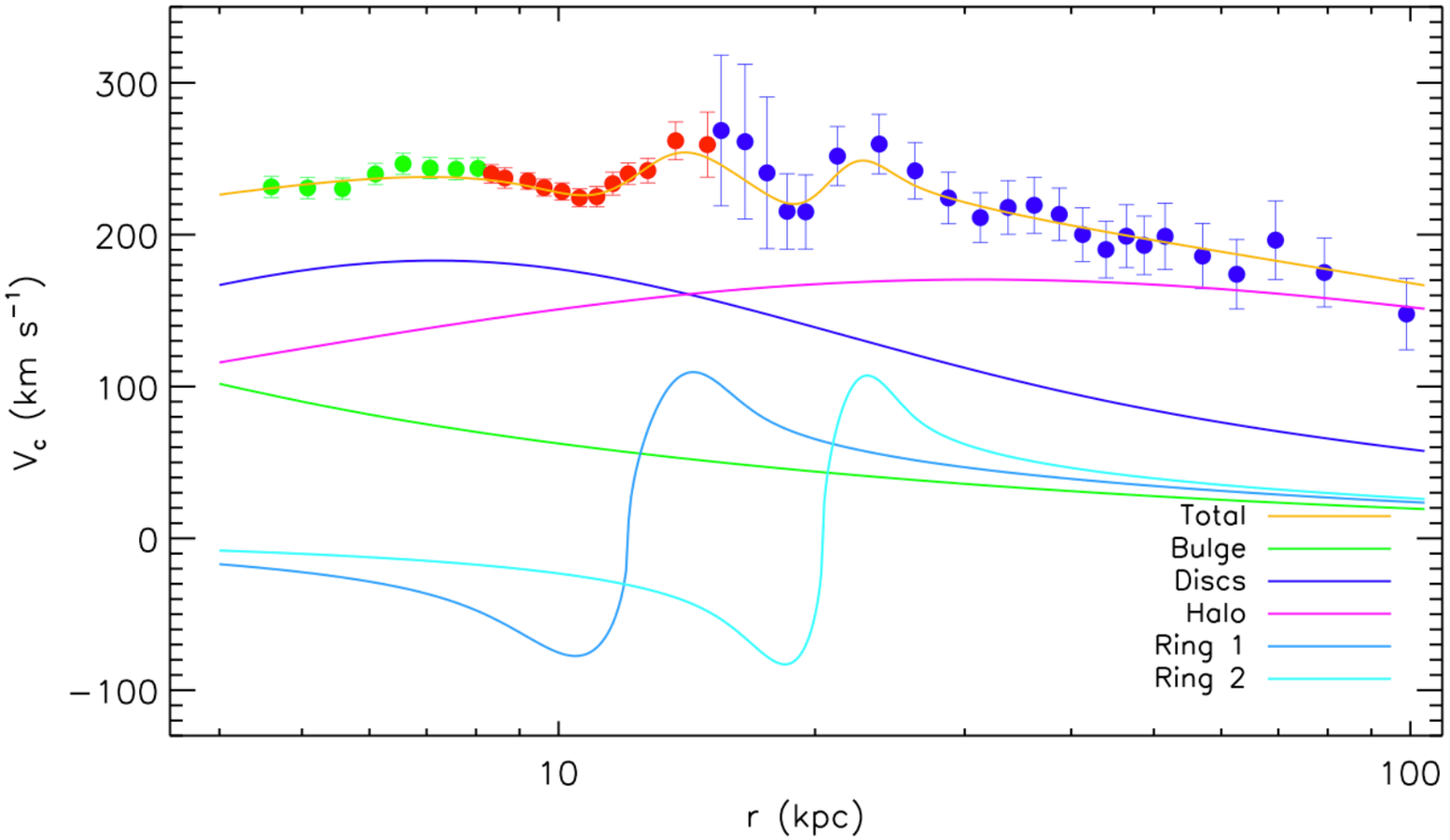

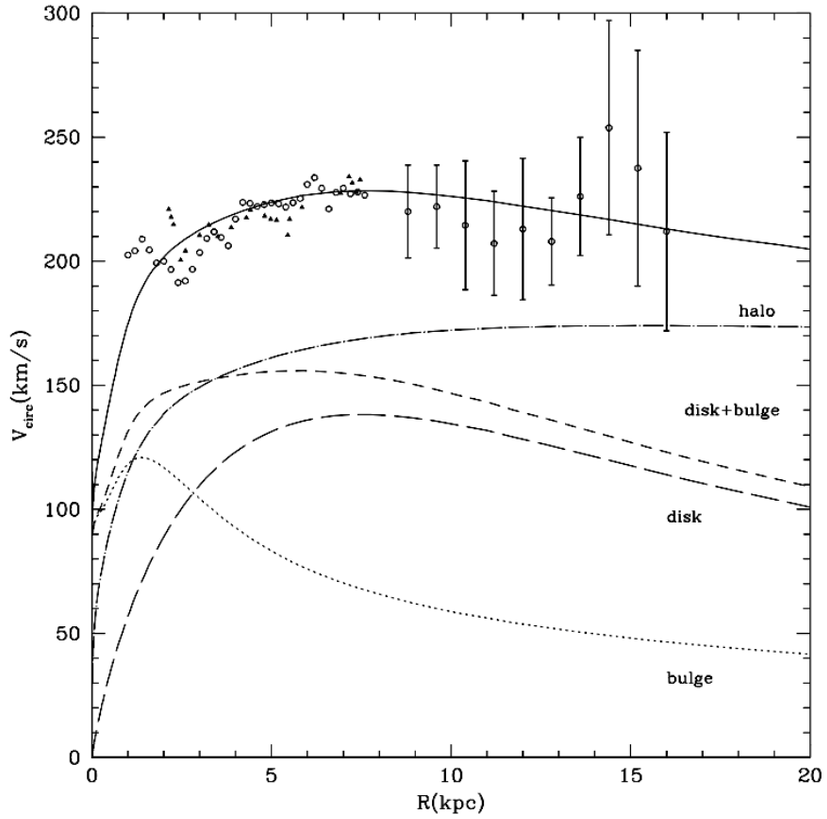

Circular velocity curve at large distances.
It is rather flat for radii 5-30 kpc . At larger distances it starts to gradually decline in agreement with modern cosmological models.

More recent results may indicate presence of rings at 15kpc and 22kpc though this still needs to be confirmed

Mass profile of the Milky Way (symbols)
Curves show analytical models that fit the data.

The very central region is probed by motions of stars and gas. The central black hole dominates at radii <10pc.

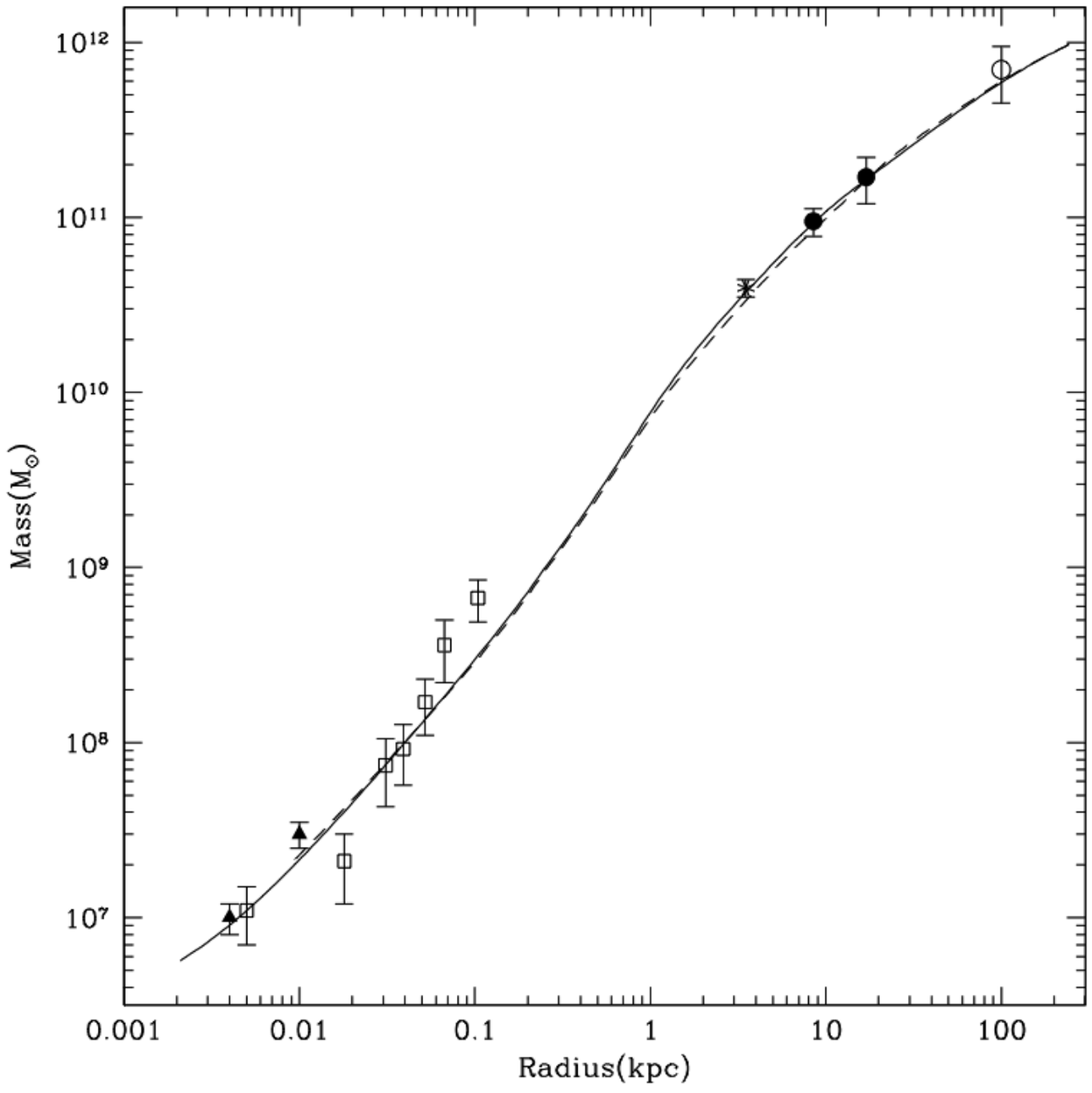

Spherically averaged density profiles of different components in the MW